NON-NUCLEAR MATERIALS COMPATIBILITY TESTING OF NIOBIUM – 1% ZIRCONIUM AND 316 STAINLESS STEEL FOR SPACE FISSION REACTOR APPLICATIONS

A Thesis
Presented to
The Academic Faculty

by

Omar R. Mireles

In Partial Fulfillment
of the Requirements for the Degree
Masters of Science in the
Woodruff School of Mechanical Engineering

Georgia Institute of Technology
March 2004

Non-Nuclear Materials Compatibility Test of Niobium – 1% Zirconium and 316 Stainless Steel for Space Fission Reactor Applications

Approved by:

Dr. S. Mostafa Ghiaasiaan, Chairman

Dr. Michael Houts, LANL

Dr. Samuel Graham, Jr.

Date Approved: March 11, 2004

ACKNOWLEDGEMENT

This research was funded by the NASA Harriet G. Jenkins Predoctoral Fellowship Program and the Astronaut Scholarship Foundation. I would like to thank my academic advisor Dr. S. Mostafa Ghiaasiaan of the Georgia Institute of Technology, project advisor Dr. Michael Houts of Los Alamos National Laboratories, project supervisor Thomas Godfroy of NASA Marshall Space Flight Center (MSFC), Dr. Samuel Graham Jr. of the Georgia Institute of Technology, who graciously accepted to be on my thesis committee, Dr. Jack Lackey of the Georgia Institute of Technology for his consultation, as well as the members of the Early Flight Fission Test Facility at NASA MSFC. Finally, I must thank my friends and family, without whom I would not have been able to carry out and complete this project.

TABLE OF CONTENTS

LIST OF TABLES

LIST OF FIGURES

GLOSSARY (SYMBOLS OR ABBREVIATIONS)

A_o	Molecular Weight of Oxide
A_M	Atomic Weight of Metal
Ar	Argon
^oC	Degrees Celsius
EFFTF	Early Flight Fission Test Facility
GFA	Gas Fusion Analysis
HfO_2	Hafnium Oxide
He	Helium
K	constant
kW	Kilowatt
mL	Milliliters
MSFC	Marshall Space Flight Center
Pa	Pascal
NaK	Sodium-Potassium
NASA	National Aeronautics and Space Administration
Nb-1Zr	Niobium – 1% Zirconium

PO_2	Partial Pressure of Oxygen
ppm	Parts per million
PWC-11	Niobium – 1% Zirconium – 0.1% Carbon
SNAP	Systems for Nuclear Auxiliary Power
SS	Stainless Steel
T	Temperature
t	Time
TGA	Thermal Gravimetric Analysis
W	Weight Gain per Unit Area
ζ_{PB}	Pilling-Bedworth Ratio
ρ_o	Oxide Density
ρ_M	Metal Density
wppm	Weight Part Per Million
Xe	Xenon
XPS	X-Ray Photoelectron Spectroscopy

ABSTRACT

A new generation of compact and highly efficient power production and propulsion technologies are critically needed in order to enable missions outlined in the NASA space exploration initiative. Nuclear fission power technologies as part of project Prometheus are in development to meet this need. Proposed reactor concepts utilize a combination of refractory metals and stainless steels. One such refractory alloy, Niobium –1% Zirconium (Nb-1Zr), will be used because of its strength at high temperatures, neutron absorption properties, and resistance to corrosion by liquid alkali metals. One potential problem in using Nb-1Zr is that it undergoes rapid high temperature oxidation, even in low oxygen concentrations. Long-term oxidation of the niobium matrix can significantly deteriorate the mechanical properties of the alloy. This thesis reports on experimental studies of the high temperature interaction of 316 stainless steel (316 SS) and Nb-1Zr under prototypic space fission reactor operating conditions. Specifically, how the high temperature oxidation rate of Nb-1Zr changes when in contact with 316 SS in a low oxygen concentration atmosphere.

The objective of the project reported here is to determine if transport of gaseous contaminants, such as oxygen, will occur when Nb-1Zr is in contact with 316 SS, thereby increasing the oxidation rate and degrading material properties. Experiments were preformed in a realistic non-nuclear environment at the appropriate space fission reactor operating conditions. Thermal Gravimetric Analysis techniques were used to quantify results. Coupons of Nb-1Zr and Nb-1Zr wrapped in 316 SS foil are subjected to flowing

argon with oxygen concentrations between 4-15ppm and heated to a temperature of 500, 750, and 1000^{o}C for 2 - 10 hours. Experiments are conducted at the Early Flight Fission Test Facility at NASA Marshall Space Flight Center.

The experimental results indicate that a complex oxidation process, which depends greatly on temperature and oxygen concentration, takes place at the expected operating conditions. Non-linear regression techniques were applied to experimental data in order to derive correlations for the approximate oxidation rate of Nb-1Zr and Nb-1Zr in contact with 316 SS as a function of time, temperature, and oxygen concentration.

CHAPTER 1: INTRODUCTION

1.1 - BACKGROUND

Novel technologies for power production and next-generation space propulsion systems are critically needed in order to enable missions outlined in the NASA space exploration initiative. Long duration, deep space missions require compact energy generation systems capable of sustaining a reliable energy supply with little fuel and no maintenance. Nuclear fission is an excellent candidate for these missions because it possesses many of these favorable characteristics. NASA's Project Prometheus is responsible for developing fission power reactors for deep space missions, such as the Jupiter Icy Moons Orbiter (JIMO) and surface missions such as a robotic Mars Mobile Science Laboratory or a permanently manned lunar outpost (Figure 1-1).

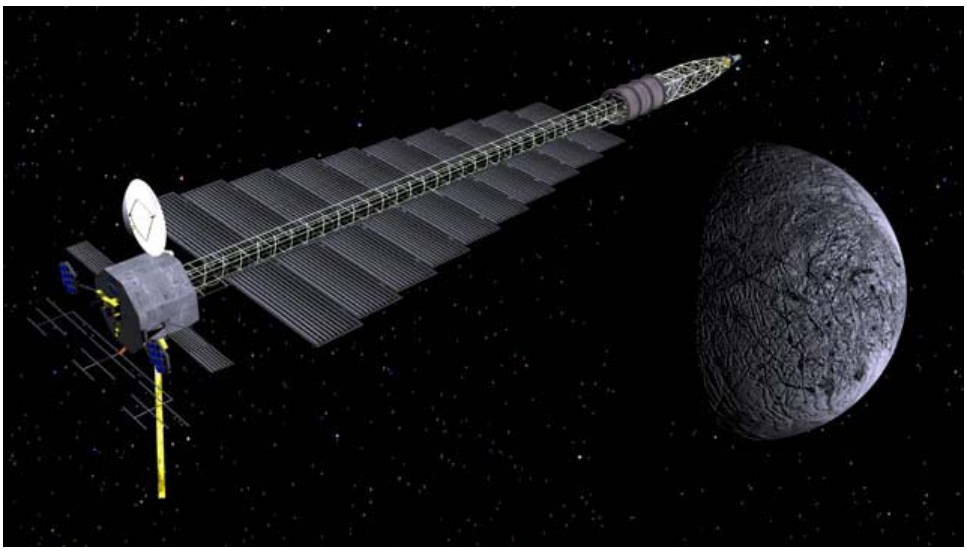

Figure 1-1: Jupiter Icy Moon Orbiter (JIMO)

Due to the obvious importance of space fission technology to the NASA strategic enterprise, project Prometheus is a high priority. A number of design, operational, and safety issues must be resolved before the application of fission reactors to space propulsion systems and surface power systems becomes a reality. These space fission power systems will need to be extremely rugged, reliable and safe. Reliability is especially important when fission reactors are utilized in long duration-manned missions.

Thermal design and thermal management are key issues for the successful development and utilization of space fission systems since safe and optimal operation of a nuclear reactor requires that the reactor operate within relatively narrow parameter ranges. Past experience with terrestrial systems has shown that careful experiments are needed in order to understand operational and safety characteristics of a nuclear reactor concept, thereby ensuring its safe and optimal operation (Sholtis et al., 1994).

Although there are numerous flight fission reactor concepts, they all possess the same basic design elements whereby thermal energy is created by the fission of a uranium-based fuel in the reactor core. Heat created in the core is then transferred to a power conversion subsystem by means of a passive or active cooling system, where the heat is converted into electrical energy. The power conversion subsystem then provides power to spacecraft components such as communications systems, scientific instruments, attitude control system, propulsive electric thrusters, etc (Figure 1-2).

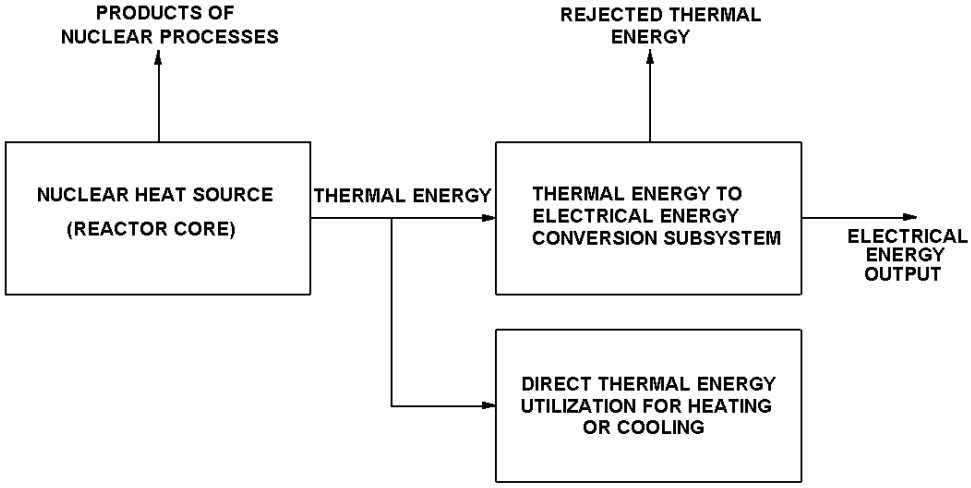

Figure 1-2: Generic space nuclear power system. *Courtesy of Angelo & Buden.*

Three types of reactors are currently under consideration by NASA. The first class of power system is a heat pipe-cooled reactor, the second is a direct drive gas cooled reactor, and the third is a liquid metal cooled reactor. The material compatibility test results found in this thesis can be applied to all three systems. In order to maintain non-nuclear testability, all experiments at this stage rely on a simulated nuclear heat source provided by electric heating elements.

Although these designs seem feasible from a systems level engineering standpoint, the reality is that practical engineering problems are not always taken into consideration. Issues that at first seem trivial eventually require an immense amount of time, effort, and resources to solve. Such issues can be avoided by subscale experiments such as the one presented here that provide experimental evidence to whether or not a concept is feasible.

1.2 - PROBLEM DESCRIPTION

Niobium – 1% Zirconium (Nb-1Zr) is intended to be used in various components of flight reactor designs including structure, heat pipes, heat pipe wick, core prism. Several components are clad with Nb-1Zr including fuel pins, beryllium control drums, and radial reflectors (Poston, 2002). Figure 1-3 depicts the cross-sectional view of the SAFE-400 reactor concept.

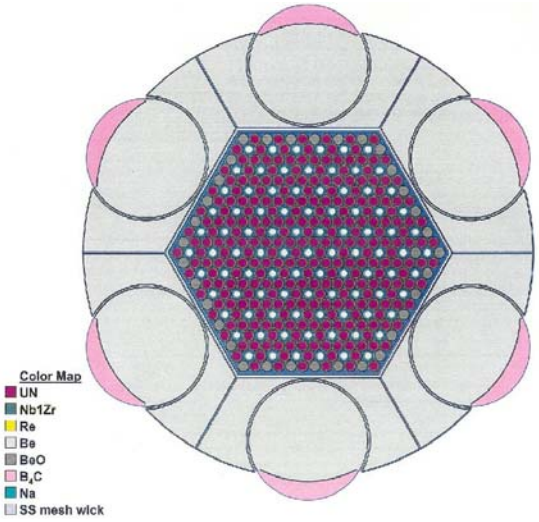

Figure 1-3. Cross Sectional View of the SAFE-400 Reactor Concept. *Image Courtesy of Los Alamos National Laboratories* (Poston, 2002)

The mass breakdown by material for this reactor concept is 158kg Nb-1Zr, 145kg UN, 125kg Be, 59kg Re, 11kg B_4C, 10kg BeO, and 4kg Na (Poston, 2002). As can seen, Nb-1Zr makes up the largest percentage. Unfortunately, Nb-1Zr is expensive and supply limited. Due to the high cost and limited supply of Nb-1Zr, it is economically beneficial to utilize stainless steel for lower temperature applications where its strength and creep

resistance properties are sufficient (Yu et al., 1993). One disadvantage of utilizing niobium alloys is that they oxidize rapidly at elevated temperatures, even in atmospheres containing very low oxygen concentrations. Low concentrations of gaseous oxygen can be provided by surface reactions with other metallic components in the power system. Utilization of dissimilar metals thus requires study of the interaction of the two under operating conditions. Stainless steels have a tendency to form surface oxide layers if not properly treated. Figure 1-4 is an excellent example of how 316 SS experiences weight loss resulting from oxidation, where in the reaction gaseous products are created.

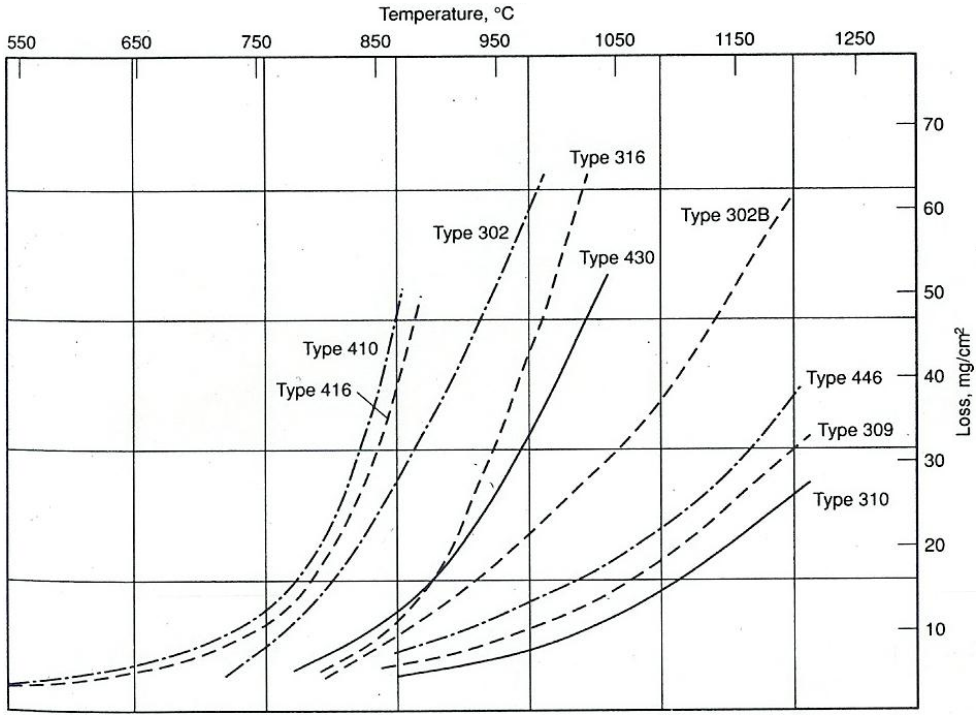

Figure 1-4: Oxidation Resistance of Several Stainless Steels as Function of Temperature. *Courtesy ASM Specialty Handbook: Stainless Steels* (ASM,1994)

Evidently, if the two metals are in contact or in close proximity, the transport of gaseous contaminants from 316 SS to Nb-1Zr components is theoretically possible during long-term operation of space fission power generation systems (Scheuermann et al., 1987). A major concern is the deposition of oxygen onto the surfaces of Nb-1Zr components, allowing the oxygen to diffuse into the material over time. The introduction of oxygen into the Nb-1Zr matrix will significantly increase the oxidation rate, thereby degrading mechanical properties of Nb-1Zr components before their design lifetime has been meet.

1.3 - EXPERIMENT OBJECTIVE

Space fission power systems materials compatibility experiments require subscale tests in order to examine the material interaction phenomena and resolve issues related to oxidation in a non-nuclear environment before advancing to component level tests, or a full-scale core. The objective of the investigation reported in this thesis was to determine if transport of gaseous contaminants, such as oxygen, will occur when Nb-1Zr is in contact with 316 SS, thereby increasing the oxidation rate and degrading material properties of Nb-1Zr. Determination of the oxidation rate of Nb-1Zr and Nb-1Zr in contact with 316 SS at prototypic flight reactor operating conditions is critical in utilizing the alloy in a flight reactor. Experiments were conducted 500, 750, and 1000^{o}C and oxygen concentrations ranging from 3 -15 parts per million (ppm).

.

CHAPTER 2: LITERATURE REVIEW

2.1 - NIOBIUM –1 % ZIRCONIUM BACKGROUND

Refractory metal alloys are typically utilized in applications where high strength at elevated temperatures is required. Extensive study of refractory metals was carried out for space nuclear power applications during the Systems for Nuclear Auxiliary Power (SNAP) program in the 1960's and the SP-100 program during the 1980's (King and El-Genk, 2000). Since liquid alkali metals are excellent heat transfer media (low density, low vapor pressure, high specific heat, high thermal conductivity, high boiling point, and a wide temperature range for the existence of liquid phase), they are excellent candidates to be used in compact thermal management systems in space fission reactors, such as sodium heat pipes or pumped sodium-potassium (NaK) loops (Keeton et al., 1987).

Niobium (previously known as columbium) is a refractory metal with a melting temperature in excess of 2230^{o}C. Interatomic metallic bonding in this metal is extremely strong, accounting for a high melting temperature, large elastic modulus, high strengths, and considerable hardness (Callister, 1999). Niobium alloys are generally divided into three categories: low, medium, and high strength. Nb-1Zr is a solid solution-strengthened alloy and is the industry standard for low strength applications. Adding 1% zirconium to niobium greatly improves its oxygen absorption resistance by removing oxygen from the niobium solution through the formation of zirconium oxide (ZrO_2) (Wah Chang, 2003). The zirconium particles also enhance strength, creep strength, and brittle failure resistance of

the alloy by creating distortions in the crystal lattice, and therefore making it difficult for dislocations to propagate through the lattice (Figure 2-1).

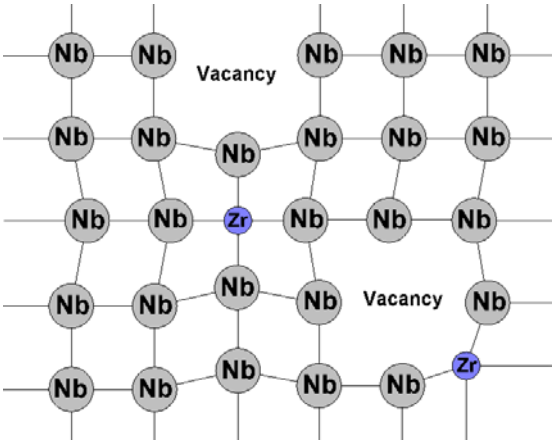

Figure 2-1: Nb-1Zr Crystal Lattice

In addition to desirable strength properties at high temperatures, Nb-1Zr has a low thermal neutron capture cross-section (Schmidt & Kania, 1987). Therefore, this alloy has traditionally been utilized in fission reactor applications where the useful properties of the alloy are needed (Refer to Appendix A for detailed material property data). The intended usage of the alloy for project Prometheus is at approximately 1000° C, where its crystal structure consists of stable β-zirconium solution in a niobium matrix (Figure 2-2).

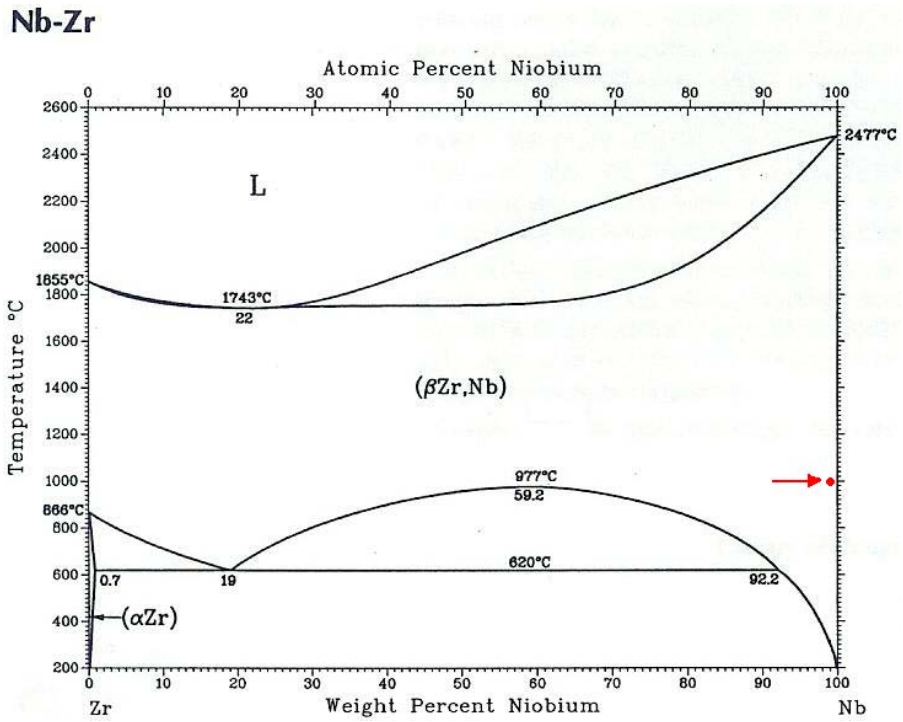

Figure 2-2: Phase Diagram of Niobium and Zirconium Alloy. *Courtesy ASM Handbook: Alloy Phase Diagrams,* (ASM, 1992)

Nb-1Zr possesses many other important characteristics as well, such as good machinability, weldability, and excellent liquid alkali metal corrosion resistance (Kramer et al., 1999).

Table 2-1: Range of Applicability for Metals and Alloys with Liquid Metals. *Courtesy ASM Specialty Handbook: Heat Resistant Materials*. (ASM, 1997)

Material	**Maximum Temperature of Operation for Nominal Corrosion (°C)**			
	Na	Li	K	Pb, Pb-Bi
Stainless Steels	600	450	600	400
Cr-Mo Steels	600	500	...	425
Ti and alloys	...	550	...	...
Nb-1Zr	900	1300	750	...

Although Nb-1Zr has been available for nearly 35 years, it has been utilized in few industries. Consequently, it is difficult to obtain reliable property data for this important alloy. In the 1960s, niobium metal was produced by high temperature vacuum sintering and carbon reduction of metal oxide. These older alloys exhibit better mechanical properties than modern (higher-purity) metals because of the higher concentrations of impurities introduced during their manufacturing (ASM, 1997). New Niobium alloys such as PWC-11 (Nb-1Zr-0.1C) have since been further developed during this period for containment of liquid alkali metals in space nuclear power systems (King & El-Genk, 2000). These alloys possess trace amounts of zirconium and hafnium, which remove oxygen from the niobium solution by the formation of ZrO_2 and Hafnium oxide (HfO_2) (ASM, 1997).

2.2 - PREVIOUS CROSS CONTAMINATION EXPERIMENT

A study by NASA Glenn in support of SP-100 was carried out, meant to determine whether or not a potential problem existed for interstitial element contamination transport to refractory metal alloy components within Brayton and Stirling power generation systems (Scheuermann et al., 1987). Auger electron spectroscopy, chemical analysis, and bend testing of Nb-1Zr specimens were utilized in that study to confirm the deterioration of mechanical properties due to the presence of interstitial contaminant transport.

Four important observations resulted from this study:

1. No reduction in ductility as a result of contaminant transfer was detected
2. No significant transport of contaminants occurred when Nb-1Zr was tested by itself.
3. Transport of carbon and oxygen was observed when other materials were present with the Nb-1Zr.
4. The observed transport of carbon and oxygen posed a potential problem.

The study revealed the extent by which Nb-1Zr specimens were contaminated by oxygen, nitrogen, and carbon. Results are shown in figures 2-3 & 2-4.

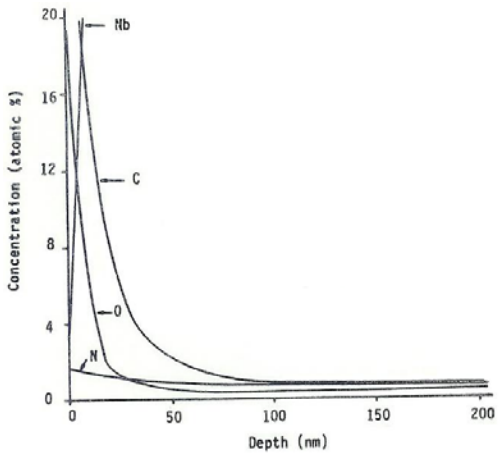

Figure 2-3: Typical Auger Analysis Depth Profile. *Courtesy of Scheuermann et al., 1987.*

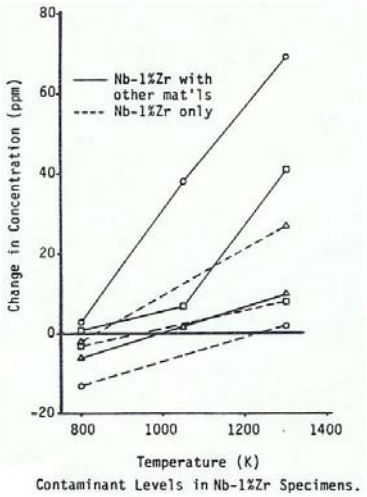

Figure 2-4: Contaminant Levels in Nb-1Zr Specimens. *Courtesy of Scheuermann et al., 1987.*

The aforementioned study by Scheuermann et al. (1987) thus provided important results. However, these experiments did not take the effect of oxygen concentration into consideration. Consequently, the results of this study can only serve as a guide for

developing a similar experimental program for project Prometheus, this time with the attention to the effect of oxygen concentration.

2.3 - Oxidation Process of Nb-1Zr

Niobium alloys support significant high temperature oxygen solubility. The formation and type of oxide scales heavily influences the oxidation process of any metal. The type of oxide scales that form is dependent on the relative volumes of both the metal and the resulting oxide. The ratio of these volumes is the Pilling-Bedworth ratio (Callister, 2000):

$$\zeta_{PB} = \frac{Ao\rho_M}{A_M \rho_O} \tag{2-1}$$

where:

- A_O = molecular weight of oxide
- A_M = atomic weight of the metal
- ρ_O = oxide density
- ρ_M = metal density

Depending on the Pilling-Bedworth ratio, the following conditions apply:

- ζ_{PB}<1, oxide film is porous and un-protective
- ζ_{PB} = 1, Protective film is formed
- ζ_{PB} >1, Compressive stresses result in the film as it forms
- ζ_{PB} = 2-3, oxide coating may crack or flake off, continually exposing a fresh unprotected metal surface

Pure niobium has a P-B ratio of 2.61, which verifies that the metal will not form a protective oxide layer (Callister, 2000).

The formation of niobium oxides both internally and externally can occur depending on exposure conditions. Unfortunately, due to the type of oxide scale formation described above, Nb-1Zr does not undergo passive oxidation where an external oxide layer acts as an oxygen diffusion barrier (DiStefano & Hendricks, 1990). Rather, the alloy experiences active oxidation where the body material reacts until it is completely oxidized. At the microstructural level, the active oxidation process can be attributed to oxygen penetration by grain boundary and bulk (vacancy) diffusion. Grain boundary diffusion in Nb-1Zr is roughly ten times larger than bulk (vacancy) diffusion, making it the more important oxidation mechanism. Nb-1Zr also has many vacancies in its crystal lattice, allowing for oxygen atoms to diffuse into the bulk of the material rapidly (Lee and Rainforth, 1994).

As oxygen diffuses interstitially into the specimen, it is preferentially absorbed by the zirconium, forming stable (monoclinic) ZrO_2 (Keeton et al., 1987). Stable ZrO_2 does not contribute to hardening, strengthening, or loss in ductility (DiStefano and Chitwood, 2001). The 1% zirconium was specifically added to niobium to tie up the diffusing oxygen into a stable compound as long as the maximum oxygen content threshold is not exceeded (Keeton et al., 1987).

$$Nb(s) + Zr(s) + 0_2(g) \overset{Heat}{\rightarrow} Nb(s) + ZrO_2(s) \qquad (2\text{-}2)$$

The oxidation front moves deeper into the matrix with continued exposure to an oxidizing environment. Once all the zirconium has reacted to form ZrO_2, further oxidation results in the interstitial oxygen reacting with niobium to form three oxide phases: NbO, NbO_2, and Nb_2O_5 (Tietz and Wilson, 1965). Each oxide phase is stable over a different temperature range, NbO_2 being prevalent at expected operating conditions of interest in this study.

$$Nb(s) + Zr(s) + 20_2(g) \overset{Heat}{\rightarrow} NbO_2(s) + ZrO_2(s) \qquad (2\text{-}3)$$

Internal oxidation of the niobium matrix results in significant reduction in ductility after a long-term exposure, thus embrittling Nb-1Zr. NbO_2 and ZrO_2 are both ceramics and therefore will fail immediately following elastic deformation, experiencing very little plasticity when compared to the originally ductile alloy (Figures 2-5 & 2-6) (Barsoum, 1996).

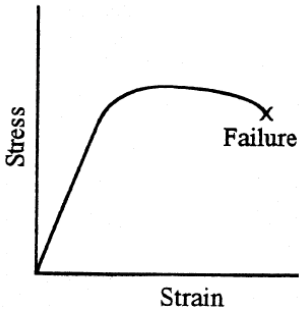

Figure 2-5: Stress strain curves for ductile materials

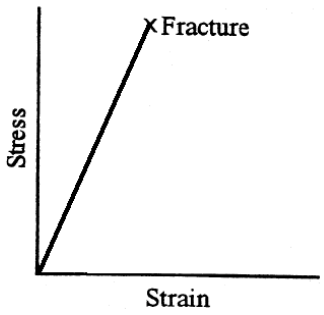

Figure 2-6: Stress strain curves for brittle materials

Ceramics typically have a low fracture toughness (K_{IC}), accounting for the brittle failure behavior of oxidized Nb-1Zr. As a result of oxidation of the niobium matrix, strength of a component is diminished due to the reduction in the effective load-bearing cross-sectional area (Lee and Rainforth, 1994).

2.4 - OXIDATION RATE

Characterizing the oxidation rate (e.g. rate of oxide film thickness increase) under prototypic operating conditions is critical for the design of systems that utilize Nb-1Zr. For metals that undergo active oxidation, the oxidation rate is linear (Callister, 2000). Studies have demonstrated that the oxidation rate of niobium alloys is parabolic from 200 to 375°C and linear from 400 to 1200°C (Tietz and Wilson, 1965). The oxidation rate is determined by measuring weight gain as a function of time (Callister, 2000). This relationship is expressed by:

$$W = kt \tag{2-4}$$

where:

- W = weight gain per unit area
- k = constant
- t = time

Oxidation rate is dependant on various parameters including the oxygen diffusion and deposition rates, temperature, gas volume to surface area ratio, surface condition, etc.

The oxidation rate of Nb-1Zr is particularly sensitive to oxygen concentration and temperature, increasing rapidly above 500^{o}C (Tietz and Wilson, 1965). However, the oxidation rate is not time sensitive, meaning that temperature and oxygen concentration are the primary oxidation mechanisms. In previous experiments, the oxidation rate at 650-900^{o}C has been determined to be 2-8 x10^{2} mg cm^{-2} h^{-1} (DiStefano and Chitwood, 2001).

2.5 - MECHANICAL PROPERTIES OF OXIDIZED NB-1ZR

Once oxidized, the mechanical properties of Nb-1Zr can vary widely depending upon temperature, partial pressure of oxygen, exposure time, material grain size, and component geometry. There are ways to mitigate these effects. Since the process is temperature dependent, reducing the operating temperature will result in a reduced oxidation rate. Significant loss of ductility should occur only to the locations where dissolved oxygen is present in the niobium matrix below the oxide film. Internal oxygen concentrations as a result of the metal manufacture process play a major role in the internal oxidation of Nb-1Zr (DiStefano and Chitwood, 2001). Component geometry influences mechanical properties of oxidized Nb-1Zr due to varying surface area to volume ratios, as well as section thickness to surface area ratios.

Experimental tests have established baseline data on various mechanical properties of Nb-1Zr as a function of temperature, oxygen concentration, time, and fabrication process (DiStefano and Chitwood, 2001, Kramer et al., 1999). One specific subject of interest is the determination of the effect of small concentrations of oxygen on the mechanical

properties of Nb-1Zr at elevated temperatures In a study by Kramer et al. (1999), Nb-1Zr specimens were exposed to high temperature in either vacuum or argon gas environment containing low concentrations of oxygen (5-15ppm), and were tensile tested after exposure. The data showed only minor variations in tensile strength, yield strength, and percent elongation measurements as a function of time (100-1000 hours) and temperature. In addition, there was no major differences in properties between machined specimens and specimens produced by wire electrode discharge machining. However, data obtained from specimens that had undergone experiments in various concentrations of oxygen displayed an increase in tensile strength with corresponding decrease in percent elongation, essentially increasing the brittleness of the material. This trend was observed in specimens exposed to as little as 5ppm of oxygen at an operating temperature of 1000^{o}C (Kramer et al., 1999).

These material properties correlate well with tests preformed by DiStefano and Chitwood which, also show that the oxidation of Nb-1Zr is dependent on variations in oxygen concentration, temperature, and fabrication history/microstructure (DiStefano and Chitwood, 2001). Even under vacuum or inert gas conditions, high temperature oxidation is a major concern since even low partial pressures of oxygen ($<10^{-3}$ Pa) can result in significant embrittlement of Nb-1Zr (DiStefano and Chitwood, 2001).

A summary of the results from experiments preformed by Kramer et al. (1999) and DiStefano and Chitwood (2001) is provided in Table 2-2.

Table 2-2: Mechanical Properties of Oxidized Nb-1Zr

Oxygen Concentration (ppm)	Temp (°C)	Time (hours)	RT Tensile Strength (MPa)	Elongation (%)	Data Source
15	925	0	379.21	24	K et al.
15	925	25	655	1.3	K et al.
15	925	75	572.26	0.7	K et al.
15	925	150	544.69	0.1	K et al.
150	1000	100	370	11	D & C
310	1000	100	444	11	D & C
650	1000	100	671	2	D & C
1200	1000	100	863	0	D & C
2100	1000	100	949	0	D & C
3260	1000	100	827	0	D & C
K et al.: Gauge: 2.5cm x 0.63 cm, Grip: 1.6cm x 1.6cm, WT=0.5mm D & S: Gauge: W=1.5mm, L=7.6mm, WT=0.5mm					

2.6 - OXIDATION PREVENTION

To avoid oxidation resulting from improper production, the fabrication of Nb-1Zr must be done in a hard vacuum, followed by sufficient oxygen reduction with carbon to ensure that only minimal amounts of interstitial oxygen is present in the crystal lattice. Reactor grade Nb-1Zr has 150-weight ppm oxygen, which has shown to be adequate in reactor applications. Furthermore, to reduce the chance of oxidation during manufacturing and application, processes such as machining, welding, heat-treating, testing, storage, and launch should be preformed in a reducing atmosphere. If the reactor design calls for a low oxygen environment (e.g. inert gas or vacuum) during operation, then the primary source of oxygen is significantly reduced. However, even moderate amounts of interstitial oxygen

in the Nb-1Zr matrix will lead to oxidation, most likely resulting in the reaction of a significant percentage of the zirconium dopant.

Research in improving the oxidation resistance of niobium alloys from external oxygen sources has focused on coatings (ASM, 1997). Niobium and its alloys can be coated for protection against high oxidation. During the Apollo program methods to apply slurry coatings of aluminides and silicides to niobium alloys were developed (see figure A-3). These coatings are reliable and display excellent cyclic performance characteristics without significant mechanical property deterioration. Approximately 0.08 mm of slurry is applied to the surface followed by vacuum heating to about 1300 to 1400^{o}C to facilitate reaction bonding and diffusion (ASM, 1990). Today, the primary niobium alloy coating utilized is Si-20Cr-20Fe. The coating is applied using powder suspended in nitrocellulose lacquer combined with a thermotropic gelling agent. (ASM, 1997).

Although improvements in high temperature oxidation resistance as a result of slurry coatings demonstrate great promise, they do have disadvantages. Coated niobium alloys display reductions in strength and ductility, higher radiative emissivity, and increased weight. The application of a coating requires the elimination of sharp edges from component design, which evidently limits certain component geometries. It is not recommended that these coated niobium alloys be spot welded or riveted (ASM, 1990). The neutron absorption and scattering characteristics of elements in the coatings are well characterized. However, the mechanical behavior of the coatings (swelling, flaking, etc.) during irradiation at temperature in a prototypic environment has not been investigated.

2.7 – SUMMARY

The oxidation rate of Nb-1Zr must be well understood before Nb-1Zr can be utilized in space flight reactors. Oxidation of Nb-1Zr is a complex process and is heavily dependent on temperature, oxygen concentration, exposure time, material grain size, fabrication history, and component geometry. Due to the high operational temperature (in excess of 1000^{o}C) some oxidation will occur, even if the oxygen concentration is maintained at very low levels. A potential source of oxygen and other gaseous contaminants can be the 316 stainless steel used within or near the reactor core. A major and unresolved question is what is the oxidation rate of Nb-1Zr and Nb-1Zr in contact with 316 SS at prototypic reactor operating conditions?

The generally expected change in mechanical properties of Nb-1Zr resulting from oxidation include: increased weight gain, increased component thickness, reduced percent elongation, reduction in ductility, increase in tensile strength, and an overall increased in embrittlement. Although these trends can be expected, their individual extent during the oxidation process is unknown. Data for specific applications are thus required, even when somewhat similar experimental results are available in the literature (DiStefano & Chitwood, 2001). In order to complete the materials compatibility tests we must create the prototypic operating conditions that we expect Nb-1Zr to experience in a space flight reactor. These conditions include a temperature of 1000^{o}C, external oxygen concentration of less than 15ppm ($PO_2 \leq 10^{-3}$ Pa), and exposure time. Reactor exposure time is 100,000 hours, however, useful baseline data is required immediately (2-10 hour tests).

CHAPTER 3: METHODOLOGY

3.1 - THERMAL GRAVIMETRIC ANALYSIS

The primary objective of this investigation is to determine the oxidation rate of Nb-1Zr and Nb-1Zr in contact with 316 SS at appropriate operating conditions. To this end, a TA Instruments Q-500 Thermal Gravimetric Analyzer (TGA) is used to determine the weight gain of Nb-1Zr specimens, as a result of oxidation, as a function of time at specific temperatures and gas flow rates (Figures 3-1 & 3-2).

Figure 3-1: TA Q-500 TGA

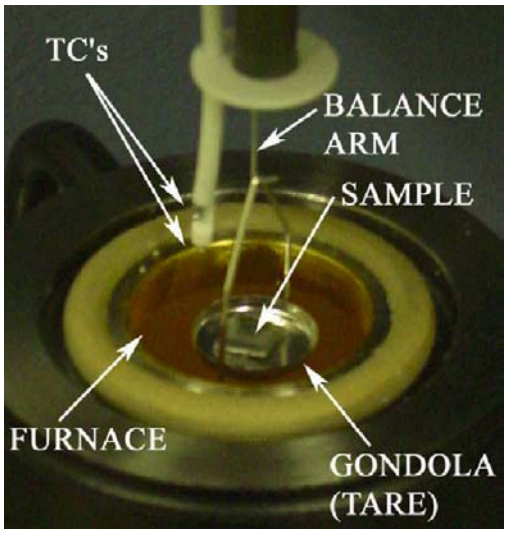

Figure 3-2: TGA Furnace Close-Up

A high purity argon purge gas is flowed through the TGA furnace in order provide some positive pressure, therefore, reducing the diffusion of the external environmental

atmosphere. The TGA uses a mass flow controller to deliver an argon purge gas via stainless steels and Tygon feed tubes. In the even of loss of flow, the TGA will discontinue sampling or fail to initiate, depending on conditions. Every function of the TGA is controlled with a data acquisition computer and TA provided software.

Upon initial experimentation with the TGA it was discovered that the furnace is unable to maintain a seal capable of preventing atmospheric infiltration into the test chamber. As a result, a Lexan glove box was built to house the TGA, allowing us to fill the box with high purity argon in order to reduce the chamber oxygen concentration (Figure 3-3).

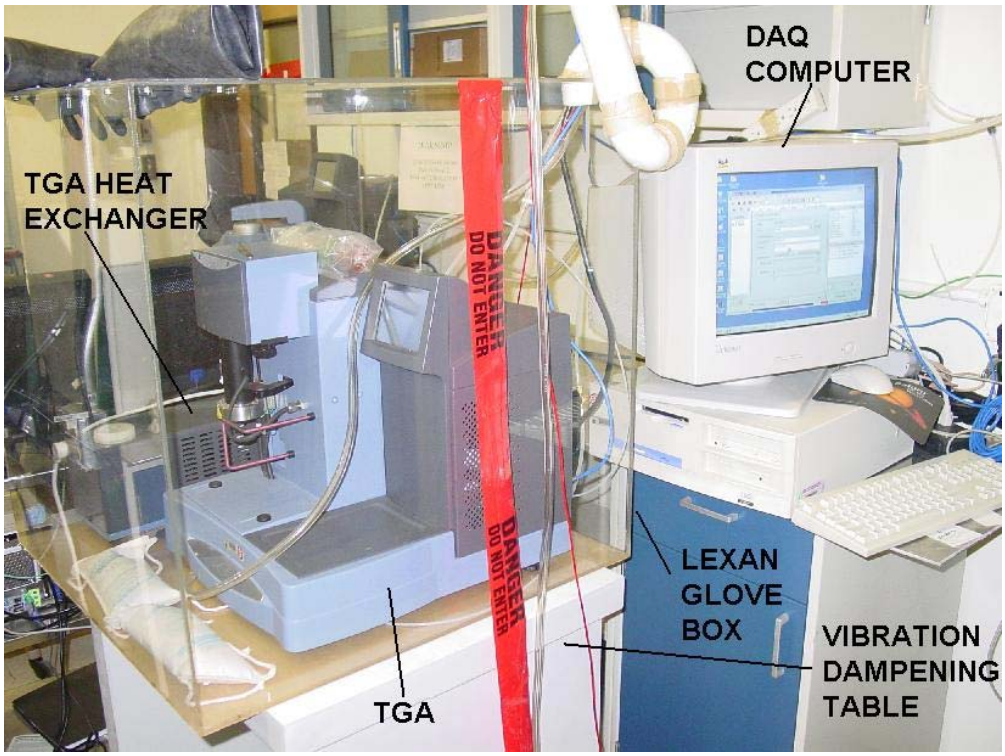

Figure 3-3: TGA in Lexan Glove Box

It was also discovered that vibrations had a tremendous effect on the weight measurement accuracy. Even walking near the instrument added a great deal of external vibrations, substantially increasing the weight measurement uncertainty. In order to minimize these external vibrations, the TGA was placed on a high mass vibration-dampening table. After implementing the mass table, scatter in the weight data was shown to decease.

An elaborate experimental set-up is required to create the appropriate low oxygen environment for the TGA to operate in. A diagram of the experiment hardware is shown in figure 3-4.

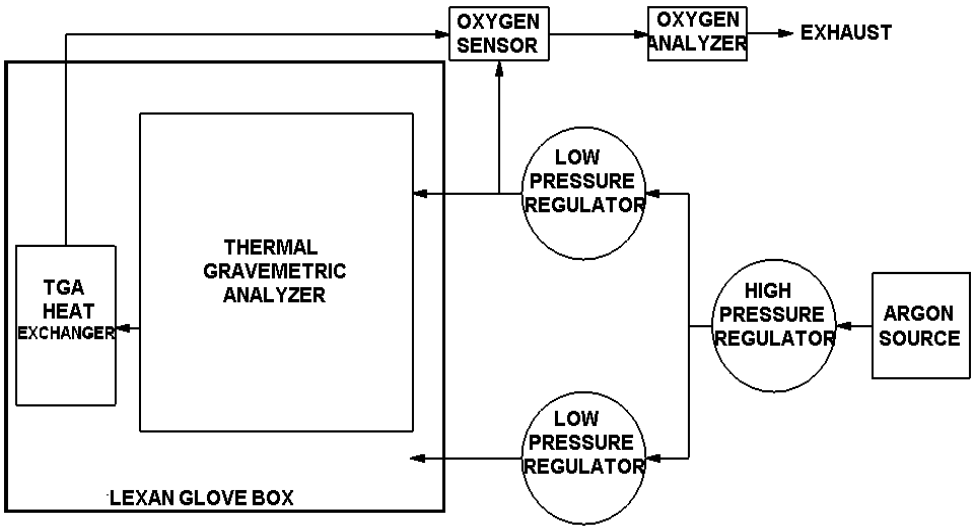

Figure 3-4: Experiment Hardware Diagram

Gaseous argon is delivered from a by a pressurized high purity argon dewer (figure 3-5) to the experimental apparatus by 6.35 mm OD 304 stainless steel lines.

Figure 3-5: Argon Dewer

Other than atmospheric oxygen, residual water vapor and oxygen found in gases provided from regular gas cylinders is the main source of oxygen contamination that can be introduced into the TGA. A dewer is designed to avoid this problem by utilizing cryogenic liquid argon to keep trace water in the tank in a solid state. Argon is liquid at temperature much lower than the freezing point of water, therefore, as the liquid argon continually boils and re-condenses inside the pressure vessel, gaseous argon is produced and settles at the top of the vessel, free of trace water vapor because the water is in solid form at the bottom of the tank. The high purity argon is supplied to the TGA, glove box, and oxygen sensor via the 6.35 mm OD 304 stainless steel lines and a series of pressure regulators (Figure 3-6).

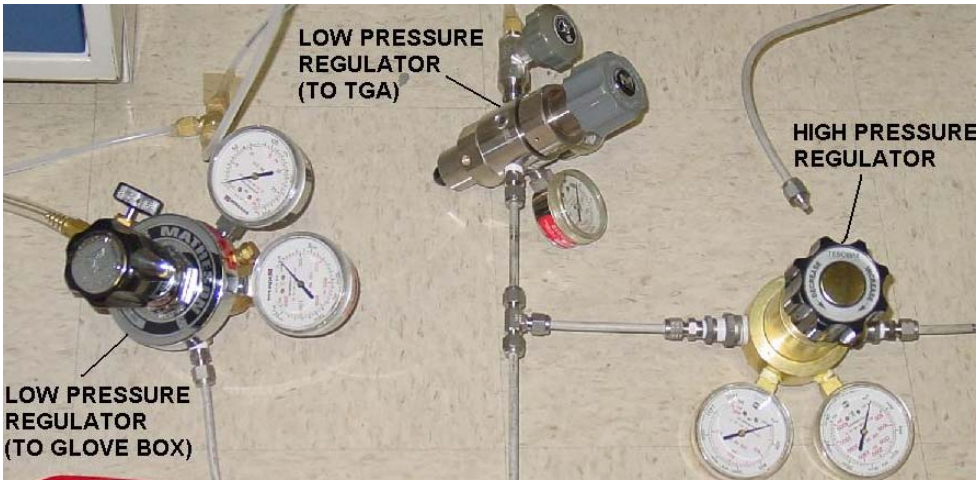

Figure 3-6: Regulators

The TGA requires an inlet gas flow rate of approximately 60 mL per second at a maximum pressure of approximately 138 kPa. However, the dewer exit pressure is approximately 2413 kPa, thus to reduce the inlet pressure to an acceptable level we employ a high-pressure regulator that steps the pressure down to approximately 1034 kPa. From here the flow gas is supplied to two low pressure regulators. One low pressure regulator supplies argon to the TGA and oxygen sensor at 1034 kPa and the other regulator provides argon to the glove box at 21 kPa but at a much high flow rate.

Before we can begin running tests using the experiment apparatus, the stainless steel gas feed lines must be heated to, and maintained at 150^{o}C for a period of 45 minutes in order to remove volatiles such as oxygen and water vapor absorbed in the metal. The bake out procedure is done in order to prevent the introduction of extraneous contamination into the

test environment of the TGA furnace. The argon is allowed to flow through the lines during this bake out period in order to carry away the vapors that form during the line heating, which are then exhausted to the atmosphere. To facilitate heating of the lines, Brisk Heat heating tape is wrapped around the inlet line, from the argon dewer to the TGA glove box, then wrapped by two layers of aluminum foil that serve as insulation (Figure 3-7).

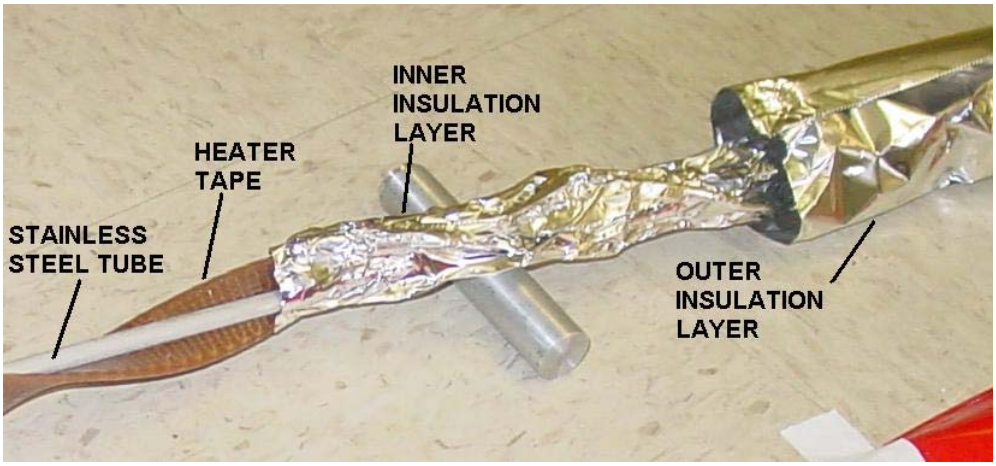

Figure 3-7: Line Heating Equipment.

The lines are elevated off the ground by insulating PEEK blocks in order to minimize heat conduction to the ground, therefore, allowing us to use a lower heater power setting and decreasing the chance of damage to the heaters. It is very important that the heater tape maximum temperature does not exceed 200^{o}C, otherwise, the heater tapes could be damaged due to the high temperatures. To monitor the temperature at the surface of the feed line, type-K thermocouples are placed at several locations along the length of feed

line from the argon dewer to the regulator assembly. These thermocouples are used in conjunction with an Omega HH509 hand held thermometer (Figure 3-8).

Figure 3-8: Omega HH509 Hand-Held Thermometer

Once the lines are volatile free they are connected to the TGA and oxygen detection equipment. Argon is allowed to flow through the lines for approximately 15 hours in order to clean away any residual oxygen that may be present from the line re-connection, bake out, and the off gassing of the stainless steel lines, also known as virtual leak. The line heating process must be repeated every time a spent argon dewer is replaced with a new dewer in order to maintain the necessary quality control standards.

A model 2100 Trace Oxygen Sensor and Analyzer by Advanced Micro Instruments Inc (AMI) is used to sample the TGA inlet and exhaust argon flows. The argon is supplied to the oxygen sensor where an oxygen sensitive membrane is housed. Oxygen chemically reacts with the membrane, which is detected by the oxygen sensor and a representative voltage is produced. The oxygen sensor supplies a DC voltage output to the oxygen analyzer, which converts the input signals to a corresponding oxygen concentration. The oxygen analyzer possesses auto-ranging response capabilities from 11 selectable output ranges, which accurately detect oxygen concentration from 0.01ppm to 25% oxygen. A digital output signal is then provided from the oxygen analyzer to a data-acquisition (DAQ) system interfaced with a RS-232 cable. The complete oxygen detection apparatus is illustrated in Figure 3-9.

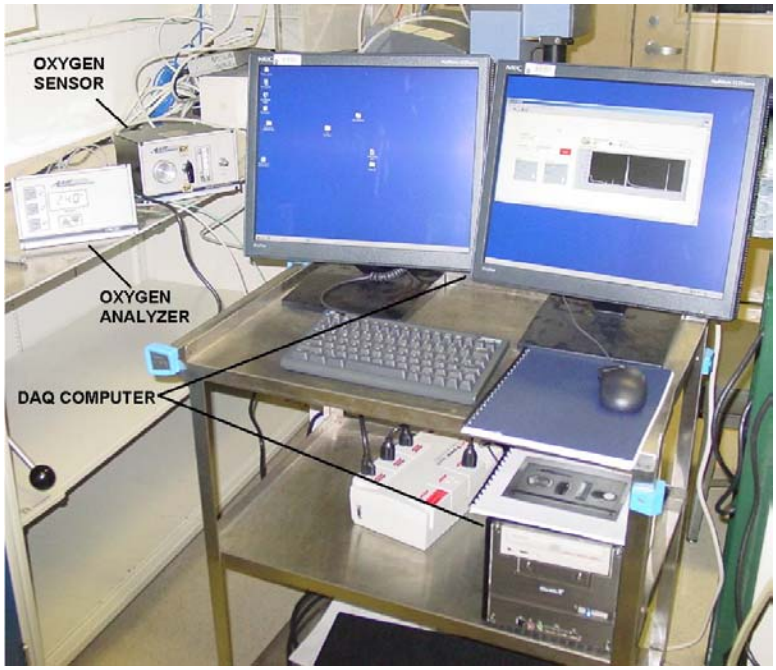

Figure 3-9: Oxygen Detection Equipment

The data acquisition computer system runs a Lab View program that samples data at user-specified rates (refer to the appendix for program specifics, figures A3 & A4). The sampling rate varies from once per second to once per minute depending on the TGA program being run. Since the inlet argon flow can be assumed to be steady, knowing the TGA exhaust oxygen concentrations provide an additional method in determining oxidation reactions occurring in the TGA furnace.

It must be mentioned that the oxygen analyzer and sensor were calibrated in air by the manufacturer. The oxygen sensor membrane is exposed to high oxygen concentrations during the air calibration and therefore becomes oxygen saturated. As a result, the sensor cannot be used to detect trace amounts of oxygen until it has been oxygen purged with a high purity flow gas. This membrane purge process takes roughly 24 hours using argon supplied from the dewer. If the sensor is exposed to air for extended periods of time this process must be repeated or the device will not have the sensitivity required to measure the trace oxygen levels of the argon flow gas.

As previously stated, argon was allowed to flow through lines leading to the TGA and oxygen sensing equipment. After purging the lines for 15 hours the oxygen concentration of the argon at the TGA inlet varied between 3-8 ppm with exhaust oxygen concentrations between 10-16 ppm. The increase of oxygen from the inlet to exhaust values can be attributed to diffusion of oxygen from the glove box atmosphere into the furnace. The argon environment of the glove box was found to have an oxygen concentration of approximately 300 ppm, which is still considerably less than air.

3.2 – SAMPLE COUPON PREPARATION

The Nb-1Zr samples are obtained by cutting several 2-3 mm long samples from tubes (OD = 3.18mm, ID = 2.86 mm) using tube cutters, then flattening these specimens into ”coupons” using two steel blocks and a press (Figure 3-10).

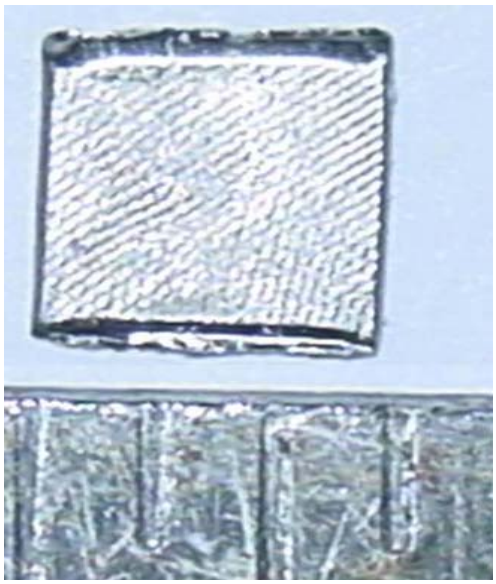

Figure 3-10: Nb-1Zr Sample Coupon

Six sample coupons are thus prepared and cleaned using isopropyl alcohol, followed by Freon leaving little to no residue. Three of the Nb-1Zr coupons were wrapped in 316 SS foil and again crushed to maximize surface contact between the coupon and the foil. The Nb-1Zr coupons and 316 SS foil are weighed separately then weighed again after combining the two using a high precision Mettler Toledo AG204 balance. Nb-1Zr coupon weights vary from 0.085 – 0.095g (refer to Table 3-1 for detailed coupon descriptions).

Before the samples are introduced into the low oxygen environment of the TGA, the coupons require the removal of volatiles and trapped air from the body material. To do this, the coupons were placed in a vacuum chamber and evacuated to approximately 1.3 $x10^{-2}$ kPa for a period of 12 hours. Next, the chamber is back filled with ultra-high purity argon. All these operations were preformed in an introduction chamber of an ultra-high purity glove box used to handle volatile liquid alkali metals (Figure 3-11 & 3-12).

Figure 3-11: Ultra High Purity Glove Box

Figure 3-12: Introduction Chamber

Once inside the ultra high purity glove box, the coupons are placed in inert plastic viles, and then the viles are then placed in a zip-lock bag and sealed (Figure 3-13).

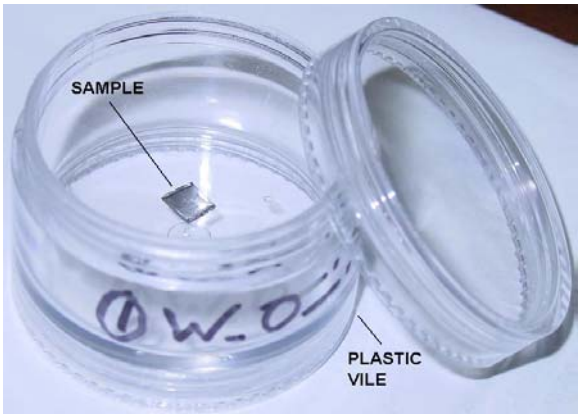

Figure 3-13: Coupon in a Vile

The ultra-high purity glove box environment conditions represented an oxygen concentration of 0.9 ppm and trace moisture dew point of –78^{o}C at slightly above atmospheric pressure. The purpose of the dual containment described above is to ensure that the samples are not re-exposed to volatile rich air when transported back to the TGA glove box. Experience with vacuum systems has shown that even minor exposure to air can result in significant absorption of oxygen and water vapor into the metal matrix. Utilizing such strict quality control standards are absolutely necessary when conducting materials research with such small coupon sizes.

3.3 – EXPERIMENT PROCEDURES

Tests were performed by subjecting coupons of Nb-1Zr and Nb-1Zr wrapped in 316 SS foil to flowing argon with oxygen concentrations of less then 15 ppm and maintained at isothermal temperatures of 500, 750, 1000^{o}C for 2-10 hours. A typical test profile is described below in detail:

1. Initiate preprogrammed TGA tare program. This program takes into account the weight of the TGA platinum gondola were the sample coupon is place so that the TGA only measures the weight change of the sample coupon.
2. Using the TGA glove box access gloves, open the appropriate coupon vile and using sterilized tweezers, carefully grab the coupon and place it in the TGA gondola. Ensure that the coupon is centered in the gondola or swinging may occur during the test as a result of external vibration and an offset coupon.
3. Set the oxygen sensor valve to sample the inlet argon flow. Set the sample rate to once per second. If oxygen concentration values are above 5 ppm continue to purge the system until this minimum threshold is achieved.
4. Initiate the LabView oxygen analyzer data-recording program. Adjust the sample rate to once per second during the purge cycle and once per minute during isothermal operation.
5. Initiate the TGA load sample gondola sequence. Make sure that the gondola is placed correctly in the sample arm to ensure a successful load.
6. Initiate the TGA raise furnace sequence.

7. Switch the oxygen sensor valve to sample the TGA exhaust flow. Initially, the oxygen concentration will spike to a rather high level, however, after several oscillations the oxygen concentration should quickly decreases to an asymptotic datum that will typically vary between 8 – 12 ppm as shown in figure 3-14. Its is critical that the isothermal test not be conducted until the oxygen concentration has reached a low and stable threshold.

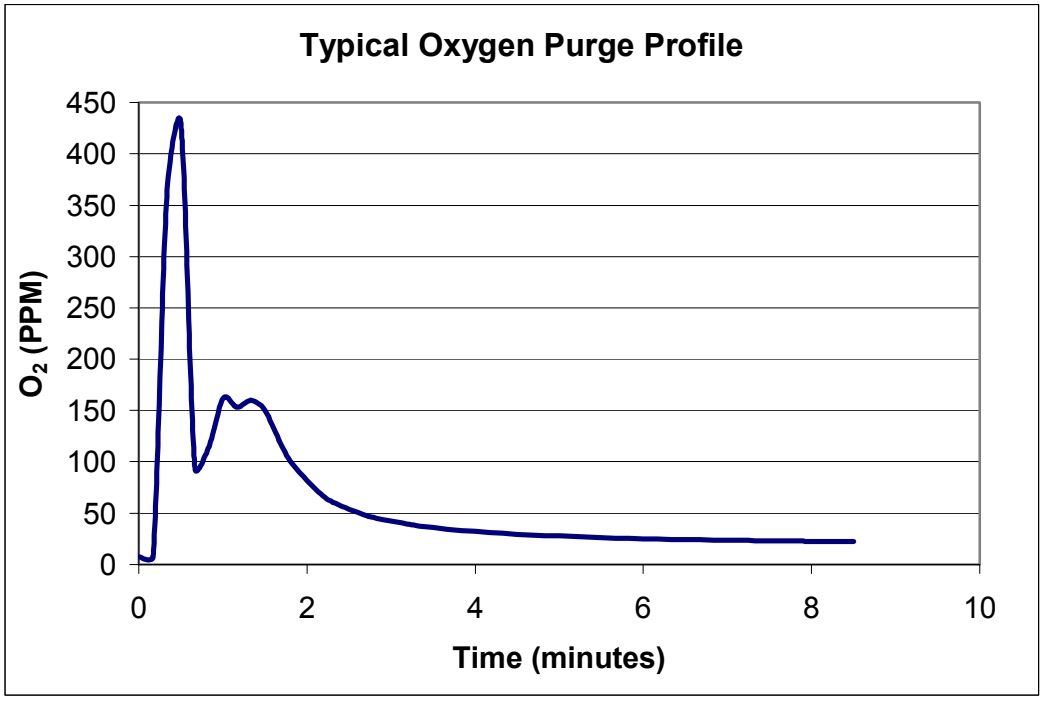

Figure 3-14: Typical Pre-Test Oxygen Purge Profile

8. Initiate the TGA line purge and test procedure program. The TGA purge and test procedure program proceeds with the following steps:

i. Increase temperature at a rate of 20°C/minute to 30 °C

ii. Maintain isothermal conditions for 20 minutes

iii. Increase temperature at a rate of 20 °C /minute to 110 °C

iv. Maintain isothermal conditions for 10 minutes. Baking out the sample coupon at 110°C before the isothermal test period removes any volatiles still adhering to the sample, such as residual water moisture.

v. Decrease temperature at a rate of 20 °C /minute to 20 °C

vi. Maintain isothermal conditions for 10 minutes

vii. Increase temperature at a rate of 20 °C /minute to appropriate operating test temperature (500, 750, or 1000 °C)

viii. Maintain isothermal conditions for 120 minutes

ix. Decrease temperature at a rate of 200 °C /minute to 20 °C

x. Maintain isothermal conditions for 55 minutes. This period allows for the samples to cool in the high purity environment before being removed from the TGA furnace and undergo additional oxidation.

xi. Initiate the TGA lower furnace routine.

xii. Initiate the TGA unload sample gondola routine.

xiii. Using tweezers, carefully remove the coupon from platinum gondola and place it in the corresponding vile.

xiv. Repeat the above procedures on each of the Nb-1Zr and Nb-1Zr wrapped in 316 SS coupons tests.

Total time to complete each test varies from 4 to 14 hours. Initially, tests were maintained at isothermal conditions for 10 hours, however, after some analysis of the data it was determined that lower times would provide similar results. Therefore, isothermal test time was decreased from 10 hours to 2 hours without significant variation in results. Table 3-1 is a detailed manifest of the experimental test matrix required to complete this investigation.

Table 3-1: Experiment Test Matrix

Test	Coupon Name	Stainless Steel Contact	Coupon Weight (mg)	Foil Weight (mg)	Test(s)	Isothermal TGA Exposure Time (hrs)	Temperature (°C)
Control	Control	N/A	95	N/A	GFA, XPS	N/A	N/A
1	W/O_.5K	NO	82	N/A	TGA	10	500
2	W/O_.75K	NO	87	N/A	TGA	10	750
3	W/O_1K	NO	94	N/A	TGA, GFA, XPS	10	1000
4	W_1K	YES	56	55	TGA	2	500
5	W_.75K	YES	54	66	TGA	2	750
6	W_.5K	YES	51	48	TGA, GFA, XPS	2	1000
7 TOTAL COUPONS 12 TESTS							

The TGA measures sample coupon weight, temperature, and time every 0.5 seconds to be used in determining the oxidation rates. Comparing oxidation rates will help us determine the influence of 316 SS on Nb-1Zr at prototypic space fission reactor operating conditions for short time durations.

CHAPTER 4: RESULTS

In order to verify the oxidation properties of Nb-1Zr stated in the literature, coupons were heated in nitrogen and air. As expected, the nitrogen, which is also a major contaminant, caused a change in the color from a silvery luster to a dark gray. When heated in air, the alloy turned white and the external layers easily flaked off, as expected (Figure 4-1)

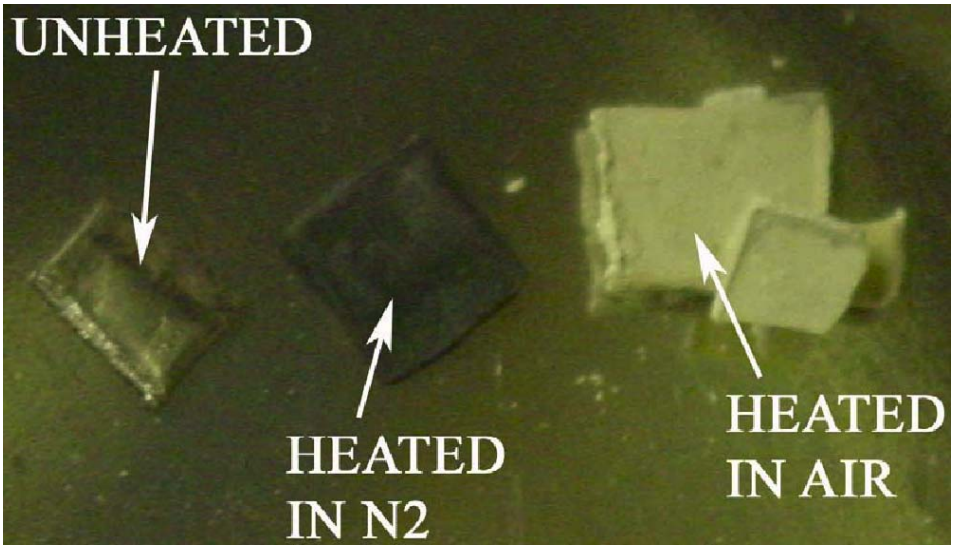

Figure 4-1: Nb-1Zr samples before and after testing in nitrogen and air.

These findings are in agreement with the hypothesis formulated by using the Pilling-Bedworth ratio, which states that Nb-1Zr heated in a high oxygen concentration environment will produce oxides that crack or flake off, continually exposing a fresh unprotected metal surface. Therefore, we can assume that active oxidation will indeed occur in the TGA furnace if a low oxygen concentration is not maintained.

Detailed weight, temperature, and oxygen concentration profiles of all six tests can be found in the appendix. The sample weight histories show that as expected, sample weight is fairly constant until a temperature of between 450-500°C is achieved, at which point rapid weight gain starts. Figure 4-2 illustrates the normalized weight rate of change of the Nb-1Zr coupons.

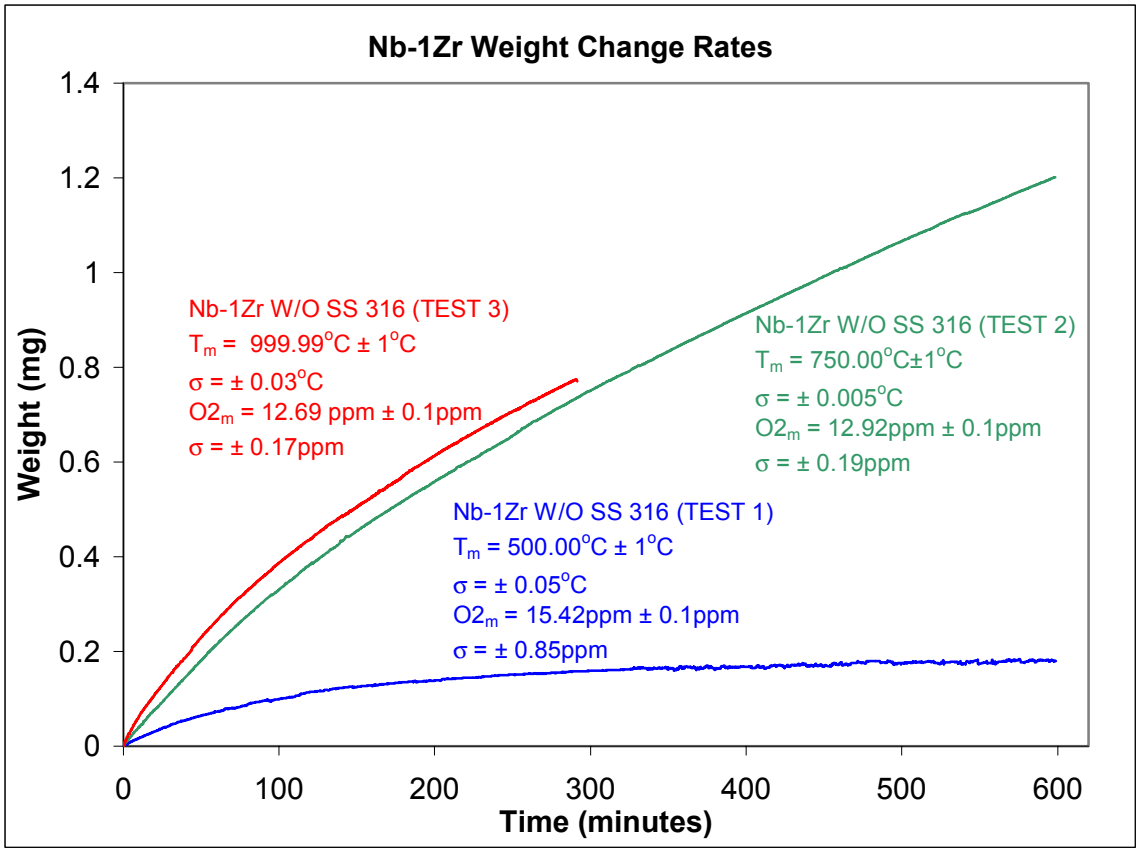

Figure 4-2: Normalized Weight Rate of Change of Nb-1Zr Coupons

The mean temperature and mean oxygen concentrations for each test were calculated to better characterize the isothermal test conditions. The results show that the rate of weight

change is proportional to temperature, in agreement with theoretical predications. However, what is not in agreement with the predictions is the non-linear oxidation rate produced in this experiment. Several literature sources stated that the oxidation rate of an active oxidizing material is not time sensitive, essentially linear (Callister, 1999). However, a square-root behavior can be noted in the data that eventually appears to reach an asymptotic limit. However, one should note that reactor grade Nb-1Zr has approximately 150wppm interstitial oxygen content, which is an order of magnitude larger than the oxygen concentration level in the external environment. Thus, interstitial oxygen is major contributor to the internal oxidation of Nb-1Zr. One can speculate that the reason for an initial non-linear behavior is that the amount of Nb and Zr available for oxidizing is initially high, accounting for the rapidly increasing the weight gain rate. However, as free interstitial and external oxygen react with the Nb-1Zr matrix, the available material for reactions to occur decreases, particularly the surface material. Thus, any further oxidation requires the diffusion of the oxygen into the Nb-1Zr body material, which is obviously a slower oxidizing mechanism than surface oxidation.

It must be emphasized the above results for Nb-1Zr oxidation rates are rather conservative because there is a continual source of oxygen to sustain the oxidation process in the experiments. The oxidation rate of Nb-1Zr components in a flight reactor operating in vacuum should eventually slow to a negligible rate as the interstitial oxygen approaches exhaustion as a result of forming oxides in the Nb-1Zr matrix. With the exception of cross contamination from other reactor materials or leaking fuel tanks, the introduction of external oxygen is unlikely. Therefore, the oxidation rates derived in these series of

investigations will provide a conservative way of overestimating the loss of effective load bearing cross sectional area when compared to the in-flight oxidation rates. Thus, flight reactor designers can use such experimentally derived oxidation rates with improved confidence that their components will meet their design lifetimes.

The normalized rate of weight change of the Nb-1Zr coupons wrapped in 316 SS is illustrated in figure 4-3. The general trend of increasing weight gain rate with temperature is again observed, although, there is much more scatter in the data.

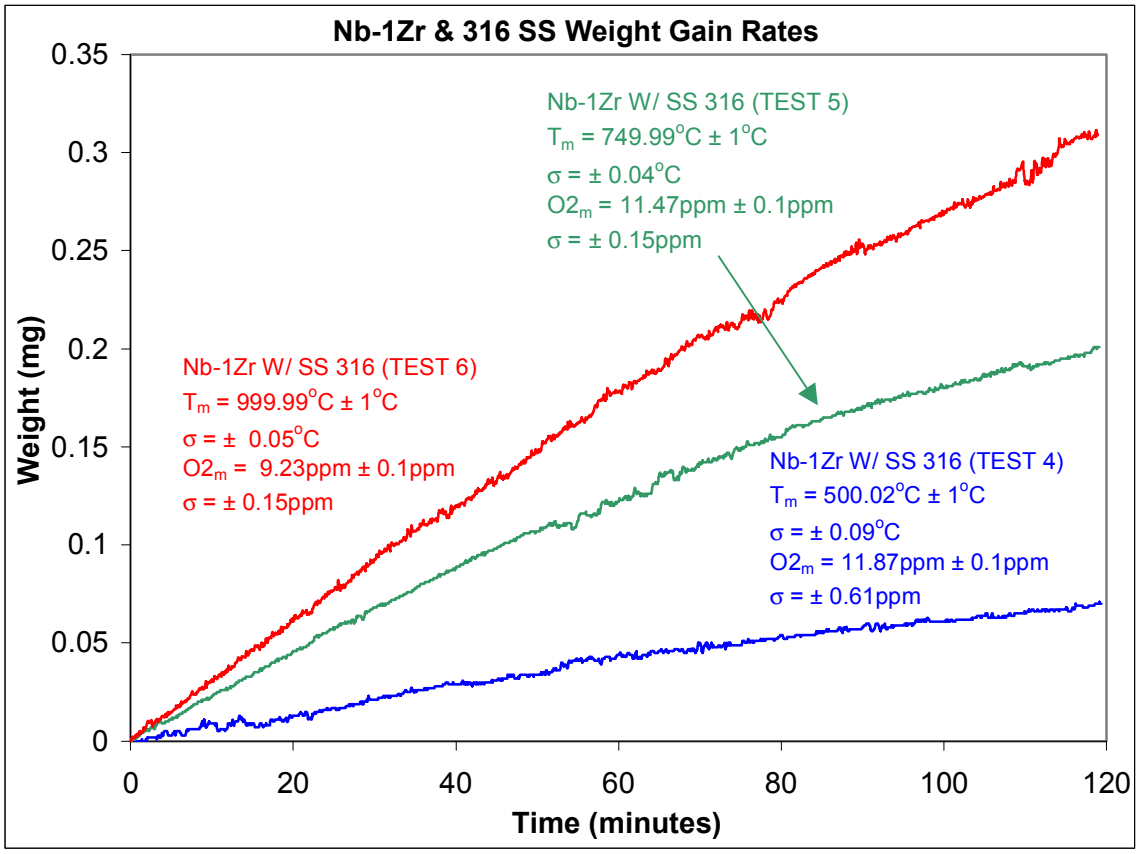

Figure 4-3: Normalized weight gain rate of change for Nb-1Zr in contact with 316 SS.

Recall that stainless steel looses weight when oxidizing at high temperature, therefore, the scatter can be attributed to the fact that a complex reaction occurs between the two metals during heating. As the samples are heated, the Nb-1Zr coupon gains weight. Concurrently, the 316 SS foil looses weight. These two competing effects lead to the alternating spikes of increased and decreased weight.

With the change of weight rates for Nb-1Zr and Nb-1Zr in contact with 316 SS known, we can now compare the weight gain rates at the corresponding operating temperatures. In figure 4-4 we illustrate the comparison the two rates at 500°C.

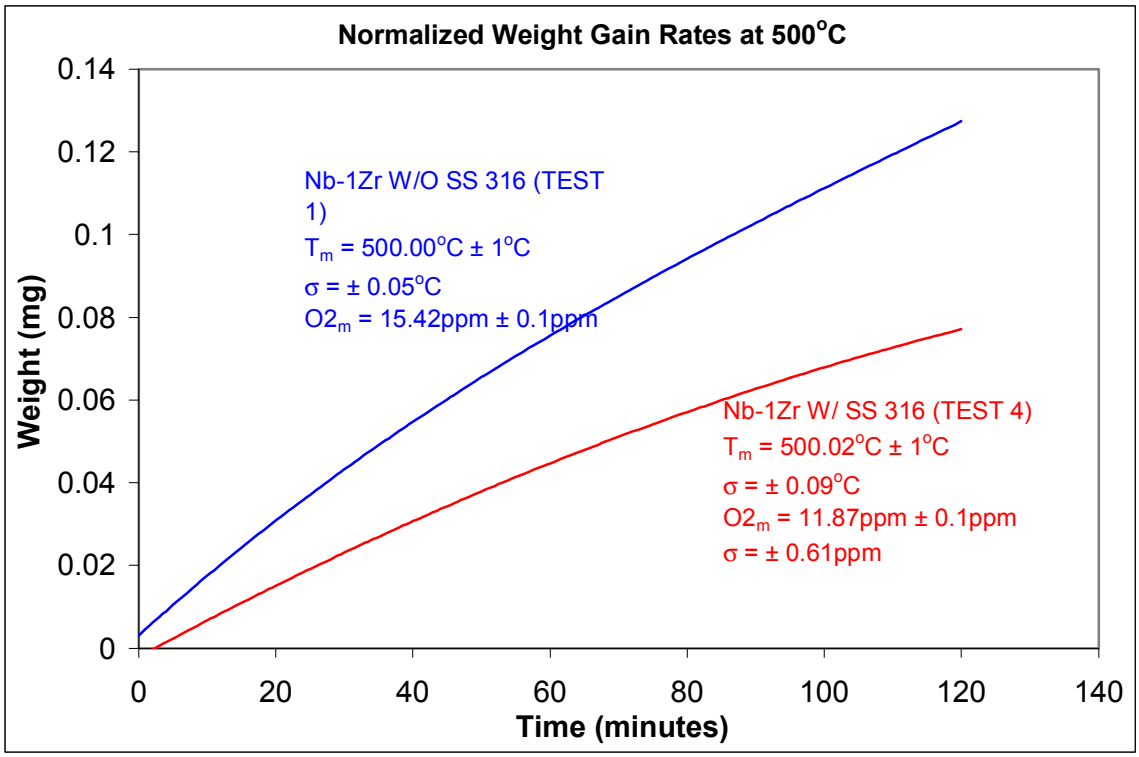

Figure 4-4: Comparison of Normalized Weight Change Rates at 500°C.

The two weight gain patterns are of course qualitatively similar. However, pure Nb-1Zr actually has a faster rate of oxidation than does Nb-1Zr wrapped in 316 SS foil. Similar trends were observed at all other temperatures examined in this study. This observation is in contradiction to our hypothesis and is problematic because we know steels loose weight when oxidized and that Nb-1Zr gains weight, therefore, there should have been gaseous transport from one sample to the other. A more plausible explanation for the lower oxidation rate for Nb-1Zr coupons wrapped in 316 SS is that the foil essentially isolates the Nb-1Zr coupon from the argon flow, which is the major source of oxygen, driving down the dominant source of for the oxidation process.

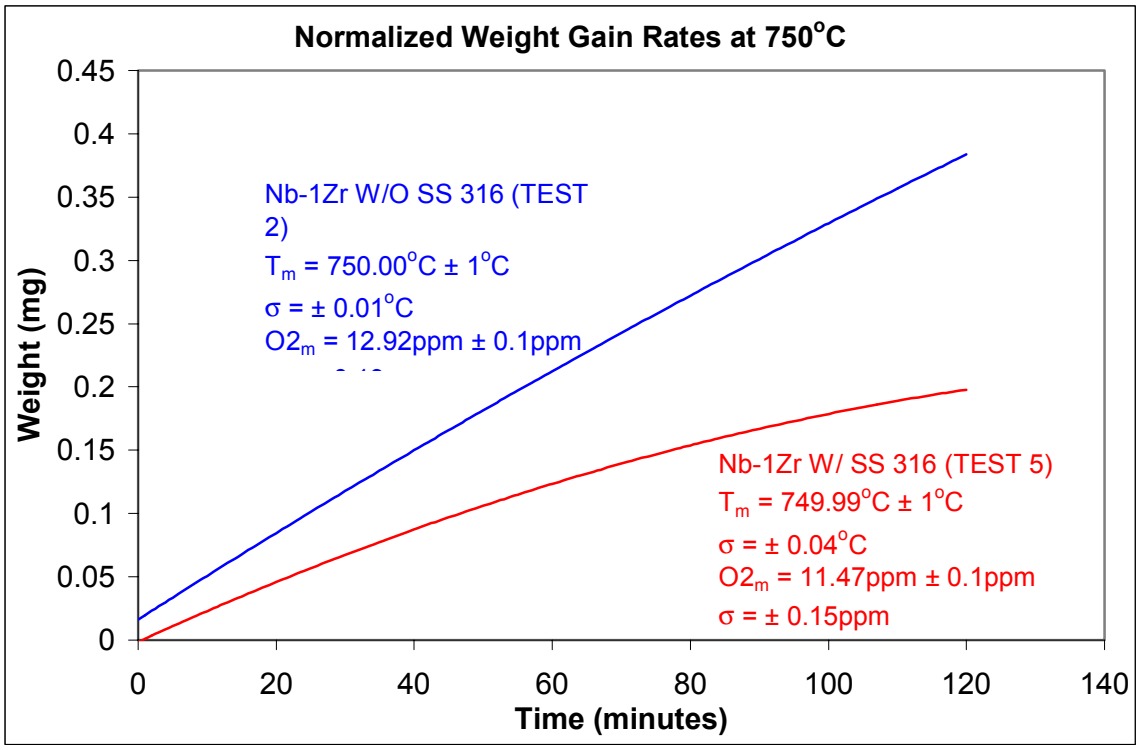

Figure 4-5: Comparison of Normalized Weight Change Rates at 750°C.

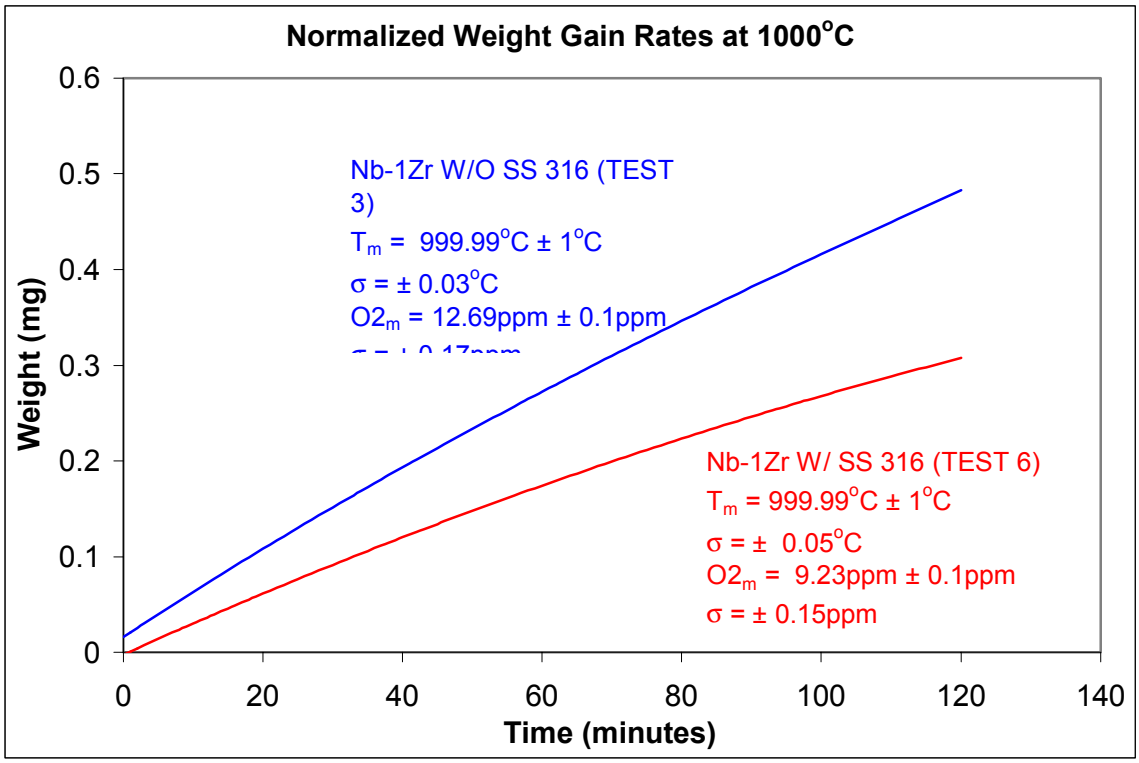

Figure 4-6: Comparison of Normalized Weight Change Rates at 1000°C.

Applying a non-linear least squares fit to the normalized data, we can then calculate a very conservative value for the oxidation rate of Nb-1Zr and Nb-1Zr in contact with the 316 SS foil at 500, 750, 1000°C, with oxygen concentrations from 3-15ppm. It is emphasized, however, that the oxidation rate calculated from any correlation derived based on data similar to these series of experiments is accurate for times from 2-10 hours and greatly overestimates weight gain for longer time durations. After all, the oxidation rates are based on experimental data for times up to 10 hours.

For design purposes, however, oxidation processes over years are typically of concern where the rate in years is extrapolated using correlations developed based on data obtained over hours, the estimations is likely to be very conservative. These non-linear regressions were created using Microsoft Excel build-in trend-line capabilities. The polynomial power was increased one order at a time until the correlation factor approached unity. The results of the non-linear regression program applied to the experimental TGA data to produce functions of oxidation rate (mg) of Nb-1Zr and Nb-1Zr in contact with 316 SS with respect to time (seconds) are shown below in table 4-1 .

Table 4-1: Oxidation Rate Non-Linear Regression Correlations

Test	Coupon	Non-Linear Regression Correlation	R^2
1	W/O_.5K	$W(t) = 1E\text{-}14t^5 - 2E\text{-}11t^4 + 2E\text{-}08t^3 - 6E\text{-}06t^2 + 0.0015t + 0.0031$	0.9982
2	W/O_.75K	$W(t) = 3E\text{-}09t^3 - 4E\text{-}06t^2 + 0.0035t + 0.0162$	0.9998
3	W/O_1K	$W(t) = 2E\text{-}08t^3 - 1E\text{-}05t^2 + 0.0048t + 0.016$	0.9998
4	W_.5K	$W(t) = -2E\text{-}06t^2 + 0.0009t - 0.0021$	0.9956
5	W_.75K	$W(t) = -7E\text{-}06t^2 + 0.0025t - 0.0013$	0.9994
6	W_1K	$W(t) = -6E\text{-}06t^2 + 0.0033t - 0.0022$	0.9992

As mentioned before, the experimentally derived values for the oxidation rate in terms of years is very high because of the continual source of oxygen being introduced into the system. Since there will be no such oxygen source in a flight reactor, these derived rates will greatly overestimate the weight gain of actual flight components. Future experiments may consider using a vacuum compatible TGA in order to produce more accurate results.

Approximate hourly oxidation rates of Nb-1Zr and Nb-1Zr in contact with 316 SS were calculated using the above correlations and are shown in table 4-2.

Table 4-2: Hourly Weight Gain of Nb-1Zr & Nb-1Zr with 316 SS

	500°C		**750°C**		**1000°C**	
	15ppm	12ppm	13ppm	12ppm	13ppm	10ppm
	W/O SS	W SS	W/O SS	W SS	W/O SS	W SS
Weight Gain per Hour (mg)	0.0756	0.0447	0.212	0.124	0.272	0.174

Table 4-2 clearly demonstrates how even seemingly negligible changes in oxygen concentration can have significant effect on the oxidation rate. This statement was also verified by tests run at similar conditions as the six sample tests in order to achieve repeatability in the data. These verification tests were on the order of one hour and as long as the isothermal temperature and oxygen concentration was maintained to similar values as the tests mentioned in this document, the weight gain rates were nearly identical.

CHAPTER 5: CONCLUDING REMARKS AND RECOMMENDATIONS

5.1 – CONCLUDING REMARKS

The oxidation rate of Nb-1Zr and Nb-1Zr in contact with 316 SS has been experimentally determined for operating times of 2-10 hours using thermal gravimetric analysis. Tests were performed by subjecting coupons of Nb-1Zr and Nb-1Zr wrapped in 316 SS foil to flowing argon with oxygen concentrations of between 3 - 15 ppm and maintained at isothermal temperatures of 500, 750, 1000^{o}C for 2-10 hours. Oxide phase types are to be measured using X-ray Photoelectric Spectroscopy and pre/post test impurity content is to be determined using Gas Fusion Analysis. Based on the available literature, physical and experimental results the following conclusions are made:

1. Nb-1Zr is an appropriate material for flight reactors. Nb-1Zr should not be used in lunar or Martian environments due to the composition of the local regolith. To mitigate oxidation strict quality control measures must be taken in order to minimize oxygen absorption by Nb-1Zr components before and during operation.
2. To avoid oxidation during component preparation, oxygen concentrations of less then 150 wppm in the body material and 10 ppm atmospheric must be maintained during material fabrication, machining, welding, assembly, testing, launch, and power generation operations.
3. Failure to meet oxygen limits may result in an relatively extensive absorption of oxygen and possibly lead to early failure of components during operation.

4. Under prototypic reactor operating conditions of 1000°C, for an approximate 3 mm x 3 mm sample coupon size, the oxidation rate of Nb-1Zr was 0.272 mg/hour. For an Nb-1Zr coupon of the same size wrapped in 316 SS foil the oxidation rate was 0.1742 mg/hour.

Designing components to be oxidation tolerant can be accomplished by accounting for a linearly decreasing effective load bearing cross sectional area as a result of oxidation. Figure 5-1 illustrates how the oxidation front decreases the heat pipe wall thickness over time, eventually leading to rupture of the wall.

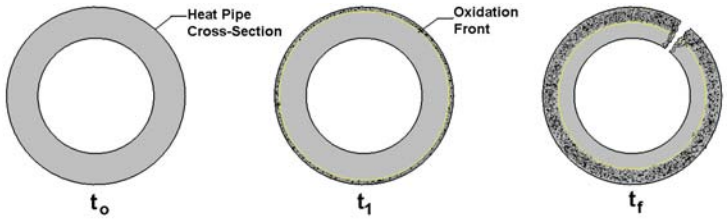

Figure 5-1: Oxidation Front leading to failure

To compensate for the oxidation process, a designer should take the minimum load bearing cross sectional area and add to it the cross-sectional area to be lost over the component's operational lifetime (calculated using the oxidation rate). The combination of both the minimum required area and the so-called "sacrificial" area will produce the new minimum cross sectional area needed to ensure that a component will meet its useful lifetime (Figure 5-2).

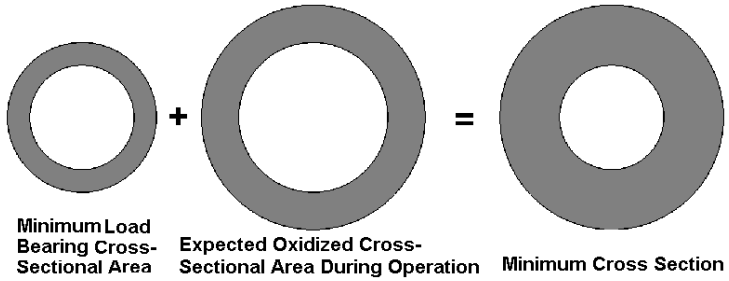

Figure 5-2: Compensating for Oxidation in the Design Phase

5.2 – RECOMMENDATIONS & PLANS FOR FUTURE RESEARCH

5.2.1 – Materials Characterization

The detailed manufacture history of Nb-1Zr is necessary before the material can be utilized in a space flight reactor application. Unfortunately, the current supplier of our Nb-1Zr material was unable to provide the manufacture history of our sample coupons. As a result a control coupon has been selected to undergo materials characterization to determine the typical impurity content and oxide phase amounts in the metal. Specifically, the oxygen, carbon, nitrogen, and hydrogen contents must be known. Samples will undergo Gas Fusion Analysis (GFA) to measure impurity content and X-ray Photoelectron Spectroscopy (XPS) to determine oxide phase content. These tests are highly recommended, and to be performed by Evans Analytical Group.

5.2.2 - Closed Cycle Gas Flow Loop Materials Compatibility Test

The gaseous contaminant transport test is to replicate the conditions in a closed Brayton power cycle in which a Helium/Xenon working fluid transfers heat from a hot Nb-1Zr heat exchanger to a 316 SS turbine. Heat is rejected to radiators before being cycled back to the heat exchanger (Figure 5-3).

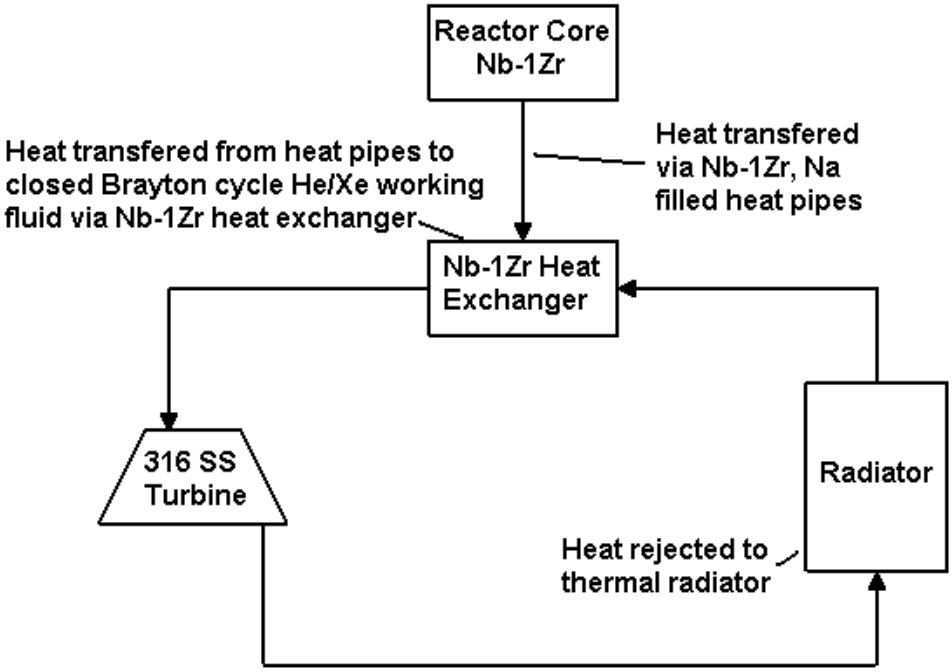

Figure 5-3: Schematic of Proposed Brayton Power Conversion Subsystem

In order to determine if gaseous contaminant transport will occur from 316 SS to Nb-1Zr in closed gas flow loops, we design an experiment that will expose Nb-1Zr sample coupons to prototypic conditions (Figure 5-4).

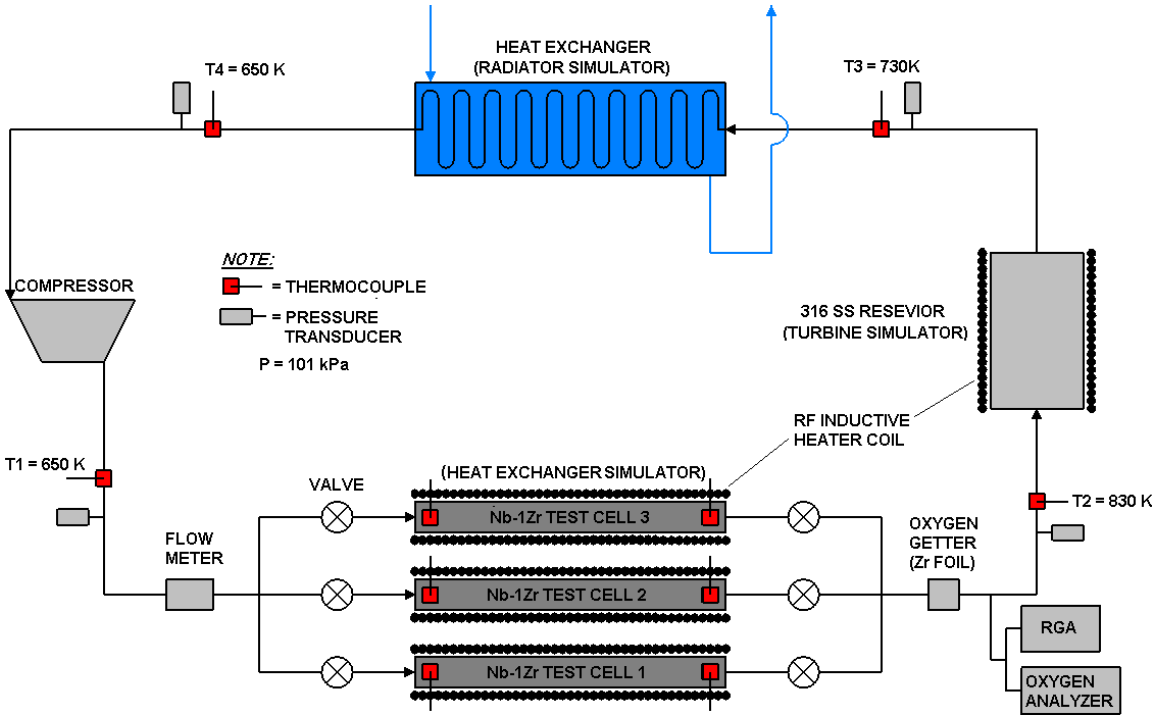

Figure 5-4: Closed Gas Cycle Materials Compatibility Test Design

The system is placed within an ultra-high purity argon glove box with an actively controlled oxygen concentration of less than 1 ppm. Next, the system is oxygen, carbon, nitrogen, and hydrogen purged and leak checked by flowing high purity helium though it, then venting the exhaust gases to the external environment. Ensuring that these extremely low gas contaminant levels are achieved will require a considerable purge time on the order of

several days. Active monitoring and control of both the glove box and the experiment flow loop is achieved by in-situ gas trace residual gas analyzers.

The experimental objective is to determine if gaseous contaminant transport will occur from 316 SS to Nb-1Zr in closed cycle gas flow loops. Conditions include temperatures between 750 – 1000^{o}C, an oxygen concentration of less then 1ppm, He/Xe flow rate, and refractory metal to stainless steel surface areas. Reactor grade Nb-1Zr coupons and wire are housed in three test cells that are heated using RF induction coils (Figure 5-5).

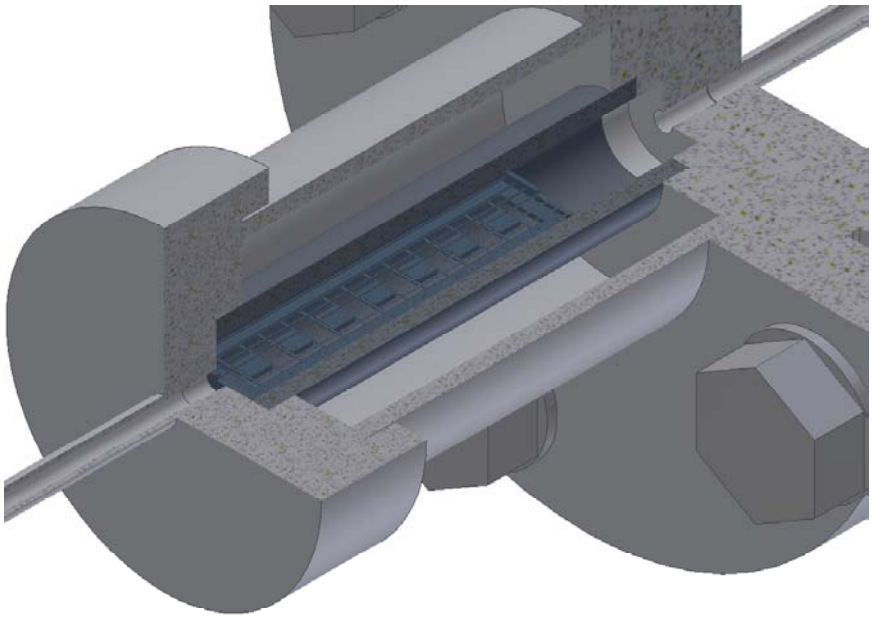

Figure 5-5: Nb-1Zr coupon Test Cell (Nb-1Zr Heat Exchanger Simulator)

A flow 316 stainless steel reservoir (turbine simulator) in addition to the flow 316 lines will provide the appropriate representative amount of stainless steel in a prototypic power conversion subsystem design (figure 5-6).

Figure 5-6: 316 Stainless Steel Reservoir (Turbine simulator)

After exposure of 1,000, 10,000 and 100,000 hours the Nb-1Zr sample coupons are subjected to materials characterization analysis such as GFA to determine the amount of contaminants absorbed, and XPS to determine what oxide phases are present and in what amounts. Mechanical testing will include tensile, ductility, compressive, and shear strength testing.

Experiments are to be preformed at the Early Flight Fission Test Facility (EFFTF) at NASA Marshall Space Flight Center (MSFC).

5.2.3 - Creep Investigations

Creep behavior studies of high-purity Nb-1Zr show marginal creep strength in terms of space fission reactor design criteria (ASM, 1997). A low creep-strength could seriously decrease system reliability and overall mission success. As a result, a variety of methods have been utilized in an attempt to increase the creep strength of Nb-1Zr. There are three ways to improve the creep strength of a material, which include adding a dispersed second phase, increasing the grain size, or adding whiskers or platelets. Nb-1Zr already has a dispersed second phase (the zirconium), whiskers may not have resistance to the radiation environment, therefore, most efforts to increase creep strength have focused on increasing grain size and adding trace amounts of other solid-solution strengtheners like carbon (ASM, 1997).

Increasing the grain size is desirable because large grains improve creep strength by reducing the grain boundary area for diffusion or sliding. One attempt to raise the creep strength of the higher purity Nb-1Zr involved increasing the grain size from 20 to approximately 80 μm. A grain size of 70 μm proved to be about 50% stronger than 20 μm material and time to 1% strain increased threefold, and similar increase was obtained for 2% strain. Unfortunately, this increase in creep strength due to a larger grain sizes have been considered marginal (ORNL, 1988). This has led to the selection of particulate strengthened Nb-1Zr, also called PWC-11 for the SP-100 program (ASM, 1997). The creep strength advantage of PWC-11 can be attributed to the presence of very fine precipitates of $(Nb,Zr)_2C$ and/or (Nb,Zr)C, which range in size from 1 to 10 μm (ASM,

1997). Creep tests of both Nb-1Zr and PWC-11 were performed at low stress levels, similar to those that may be encountered by SP-100 fuel pin claddings. As shown in figure 5-7 below, PWC-11 was found to be substantially stronger at 1075°C.

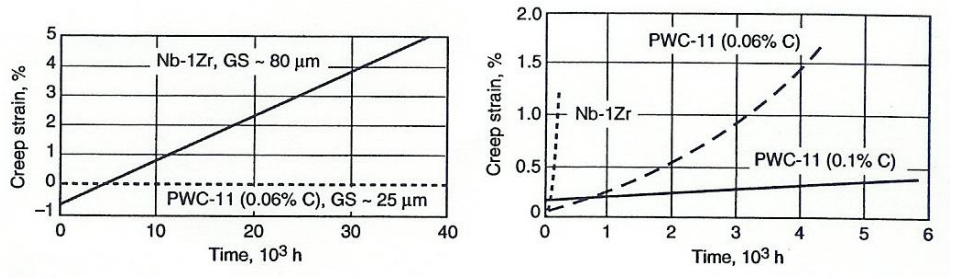

Figure 5-7: Creep Behavior of Nb-1Zr and PWC-11. *Courtesy ASM Specialty Handbook: Heat Resistant Materials*, (ASM, 1997).

Future experiments should continue to investigate the oxidation and creep properties of Nb-1Zr under expected prototypical Prometheus reactor operating conditions. These tests should include coated and uncoated alloys. Future investigations must provide sufficient data to make an educated selection.

APPENDIX

NB-1ZR PROPERTY DATABASE

Commercial Names
UNS number – Commercial Grade: R04261
Reactor Grade: R04251
Trade Name: Wah Chang WC-1Zr, Fansteel 80
Common Name: Nb-1Zr

Specifications
ASTM. B 391, B 392, B 393, B 394

Chemical Composition
Commercial Grade: 98.5 Nb min, 0.8 to 1.2 Zr, 0.0100 C max, 0.0300 N max, 0.0300 O max, 0.0020 H max, 0.01 Hf max, 0.01 Fe max, 0.005 Mo max, 0.005 Ni max, 0.005 Si max, 0.2 Ta max, 0.05 W max.
Reactor Grade: Same as commercial grade except with 0.005 Fe max, 0.015 O max, 0.1 Ta max, 0.03 W max
Consequences of exceeding impurity limits: Increasing interstitial content decreases ductility of the material.

Mechanical Properties
Tensile Strength (recrystallized): 241 MPa (Also see Table A1)
Yield Strength: 138 MPa - (Also see Table A1)
Elongation: 20% in 25.4mm - (Also see Table A1)
Shear Strength: See Table A2
Elastic Modulus: 68.9 GPa
Impact Strength: See Table A3
Creep-Rupture Properties: See figure 5, figure A2, and figure A3

Mass Characteristics:
Density: 8.59 g/cm3

Thermal Properties:
Melting Temperature: 2407°C
Coefficient of Linear Thermal Expansion: 7.54 μm/m • K at 20 to 400°C
Specific Heat: 0.270 kJ/kg • K at 20°C
Thermal Conductivity: 41.9 W/m • K at 25°C
Ductile-to-Brittle Transition Temperature: –200°C (ASM, 1997)

Electrical Properties
Electrical Resistivity: 14.7 nΩ • m at 0°C

Neutron Absorption Properties
Thermal Neutron Cross-Section: 1 barn/atom (1.1 x 10^{-28} m^2/atom)

Chemical Properties
Resistance to specific corroding agents: Especially resistant to liquid metals (also see table on liquid metals). Extensively used for liquid metal systems operating at 980 to 1205°C.

Crystal Structure
Body-Centered-Cubic (bcc)

Fabrication Characteristics
Machinability: 80% of C36000 (free-cutting brass)
Forgeability: 75% at 650 to 980°C
Formability: Extrusion: reduction ratio of 10:1 at 1065°C
Rolling: 85% reduction at 205 to 315°C and at finish. Readily formable by conventional metal-forming processes.
Weldability: Can be joined by electron beam welding, resistance welding, and gas tungsten arc welding.
Recrystallization Temperature: 980 to 1205°C
Hot-Working Temperature: 1095 to 1205°C
Stress-Relief Temperature: 1 h at 900 to 980°C

Courtesy of Properties and Selection of Nonferrous Alloys and Special Purpose Materials.

Table A-1: Effect of Temperature in the Tensile Properties of Nb-1Zr

Temperature (°C)	Tensile Strength (MPa)	Yield Strength (MPa)	Elongation (%)
20	345	255	15
1095	185	165	...
1650	83	69	...

Table A-2: Shear Strength of Nb-1Zr Rivets

Fastener Type	Diameter (mm)	Shear Strength at 20°C (MPa)	Shear Strength at 870°C (MPa)
Huck Rivet	3.18	265 300	220 220
Deutsch Rivet	3.18	240 230	180 ...
Du Pont Explosive	3.18	185 180	90 90

Table A-3: Chapry Impact Strength of Nb-1Zr

Condition	Temperature (°C)	Impact Energy (J)	Impact Fracture
Unnotched Specimens			
As Rolled	24 -73	210 180	None Partial
Stress relieved 1 h at 900°C	24 -73	175 170	None None
Recrystallized 1 h at 1205°C	24 -73	174 164	None None
Notched Specimens			
As Rolled	24 -73	>81 93	Partial* Partial
Stress relieved 1 h at 900°C	24 -73	160 129	Partial Partial
Recrystallized 1 h at 1205°C	24 -73	126 156	Partial None
*Specimen Stopped Hammer, 81J Range			

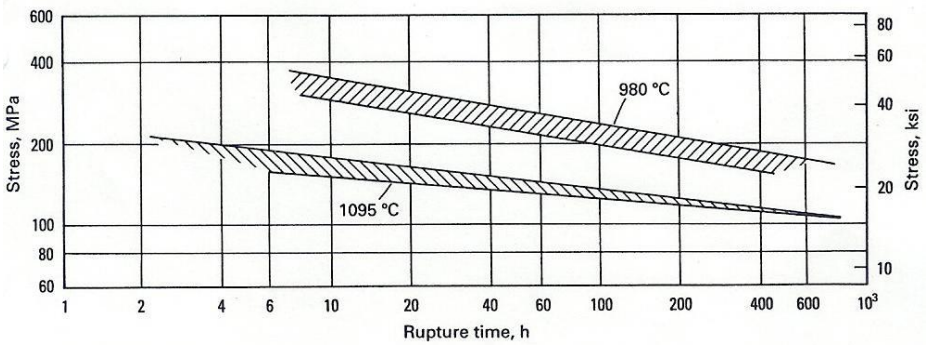

Figure A-1: Stress Rupture Properties of Nb-1Zr. *Courtesy Metals Handbook: Properties and Selection of Nonferrous Alloys and Special Purpose Materials.*

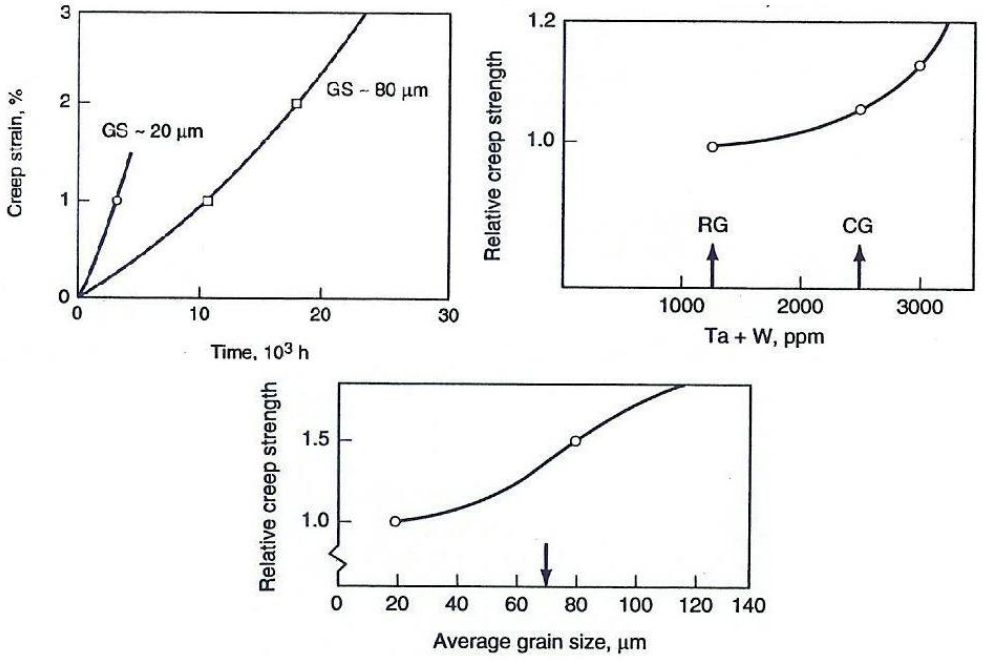

Figure A-2: Effect of Grain Size on Relative Creep Strength of Nb-1Zr. *Courtesy ASM Specialty Handbook: Heat Resistant Materials.*

Table A-4: Oxidation-Resistant Coating Systems for Niobium. *Courtesy ASM Specialty Handbook: Heat Resistant Materials*.

Oxidation-Resistant Coating Systmes for Niobium

System concept	Composition	Process
Silicide coatings		
Complex silicide multilayered	Cr, Ti, Si	Vacuum pack and vacuum slip-pack, fused slurry and pack, fluidized bed, electrophoresis, chemical vapor deposition, electrolytic fused salt
Modified silicide	Si + V, Cr, Ti	Fluidized bed
Modified silicide	Si	Pack cementation, iodine
Modified silicide	Si-B-Cr	Pack cementation, multicycle
Modified silicide	Si-Cr-Al	Pack cementation, multicycle
Modified silicide	Si + additives	Pack cementation, single cycle
Modified silicide	Si + Cr, Al, B	Pack cementation, single cycle
Silicide	Si	Chemical vapor deposition
Molybdenum disilicide	Si + Mo	MoO_3 reduction and chemical vapor deposition
Modified silicide	Si + additives	Pack cementation, fluidized bed, fused salt, slurry dip
Modified silicide	Si + additives	Pack cementation, single cycle
Liquid phase-solid matrix	Se, Sn, Al	Porous silicide applied by pack or CVD-impregnated with Sn-Al
Multilayered complex silicide	40Mo-40Si, 10CrB-10Al	Plasma spray-diffuse
Modified silicide	Si + additives	Pack cementation
Complex silicide	Si-20Fe-20Cr	Fused silicides
Complex silicide	Si-20Cr-5Ti	Fusion of eutectic mixtures
Complex silicide	Si + (Cr, Ti, V, Al, Mo, W, B, Fe, Mn)	...
Complex silicide	V-Cr-Ti-Si	Vacuum and high-pressure pack
Complex silicide	Mo-Cr-Ti-Si, V-Cr-Ti-Si, V-Al-Cr-Ti-Si, Mo-Cr-Si	Multicycle vacuum pack
Glass-sealed silicide	Si + glass	Silicide by pack cementation or CVD + glass slip overcoat
Multilayered	Mo, Ti + Si and glass	Slurry sinter application of Mo + Ti powder, pack silicide, glass slurry seal
Aluminide coatings		
Modified aluminide	Al + B	Pack cementation
Modified aluminide	88Al-10Cr-2Si	Fused slurry
Modified aluminide	Al-Si-Cr	Fused slurry
Modified aluminide	Al-Si-Cr, Ag-Si-Al	Hot dip
Multilayered systems	Fe, Cr, Al, Ni, Mo, Si, VSi_2, $TiCr_2$, $CrSi_2$, B + Al	Powder metallize + aluminum hot dip
Simple aluminide	Al	Pack cementation
Multilayered systems	Cr, FeB, NiB, Si, Al_2O_3, SiO_2, ThO_2, + Al	Electroplate dispersions in Ni + Al hot dip
Modified aluminide	Al + (Si, Ag, Cr)	Silver plate + Al, Cr, Si hot dip
Multilayered systems	Al_2O_3 + Ti + Al	(Al_2O_3 + TiH), spray-sinter + Al hot dip
Oxide-metal composite	Al_2O_3 + Al	Slurry fusion of Al_2O_3-Al mixture
Aluminide	Al + additives	Fused slurry
Modified aluminide	Al + Sn	Hot dip
Zinc coating		
Self-healing intermetallic	Zn and Zn + Al, Ti, Co, Cu, Cr, Fe, Zr, Cu, Si	Vacuum distillation and hot dip
Oxide coating		
Glass-sealed oxide	Al_2O_3 + glass (baria, alumina, silica)	Flame spray Al_2O_3 + glass slurry
Nickel-chromium coating		
Oxidation-resistant alloy	Ni-Cr	Flame spray, detonation gun, plasma arc
Chromium carbide coating		
Carbide	Cr-C	Plasma spray
Noble metal coatings		
Clad	Pt, Rh	Roll bonding and hermetic sealing
Barrier-layer-clad	Pt, Rh + Re, Be, Al_2O_3, W, ZrO_2, MgO, SiC, Hf	Noble metal clad over barrier layer-diffusion couple study
Pure metal	Ir	Fused-salt deposition

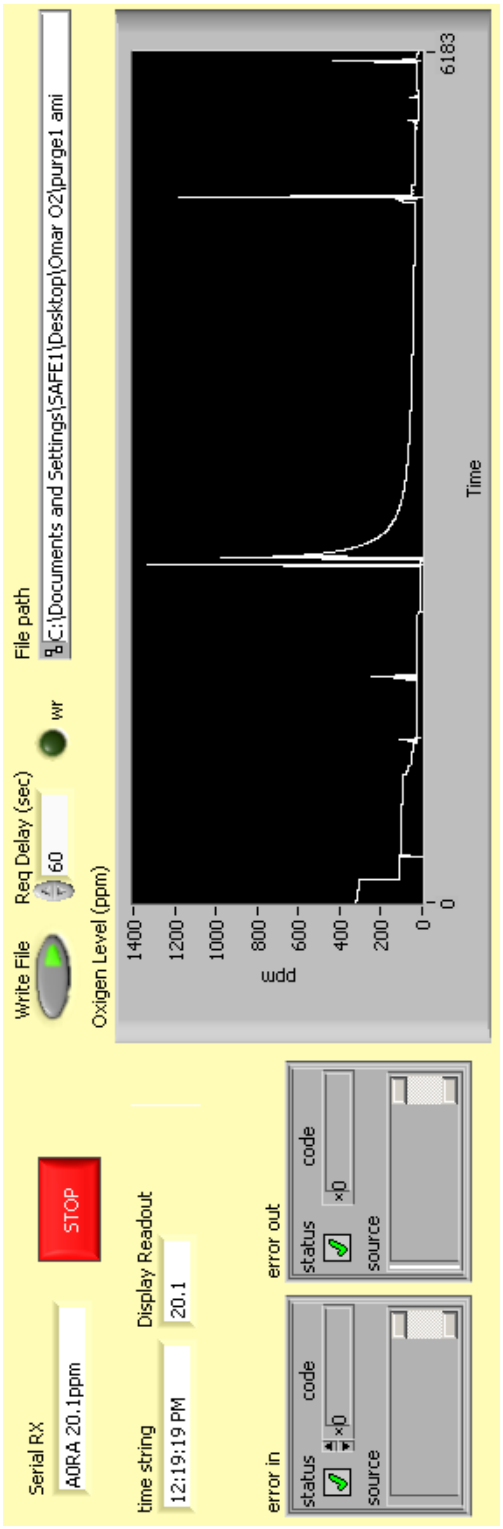

Figure A-3: O2 Detection Program Control Panel

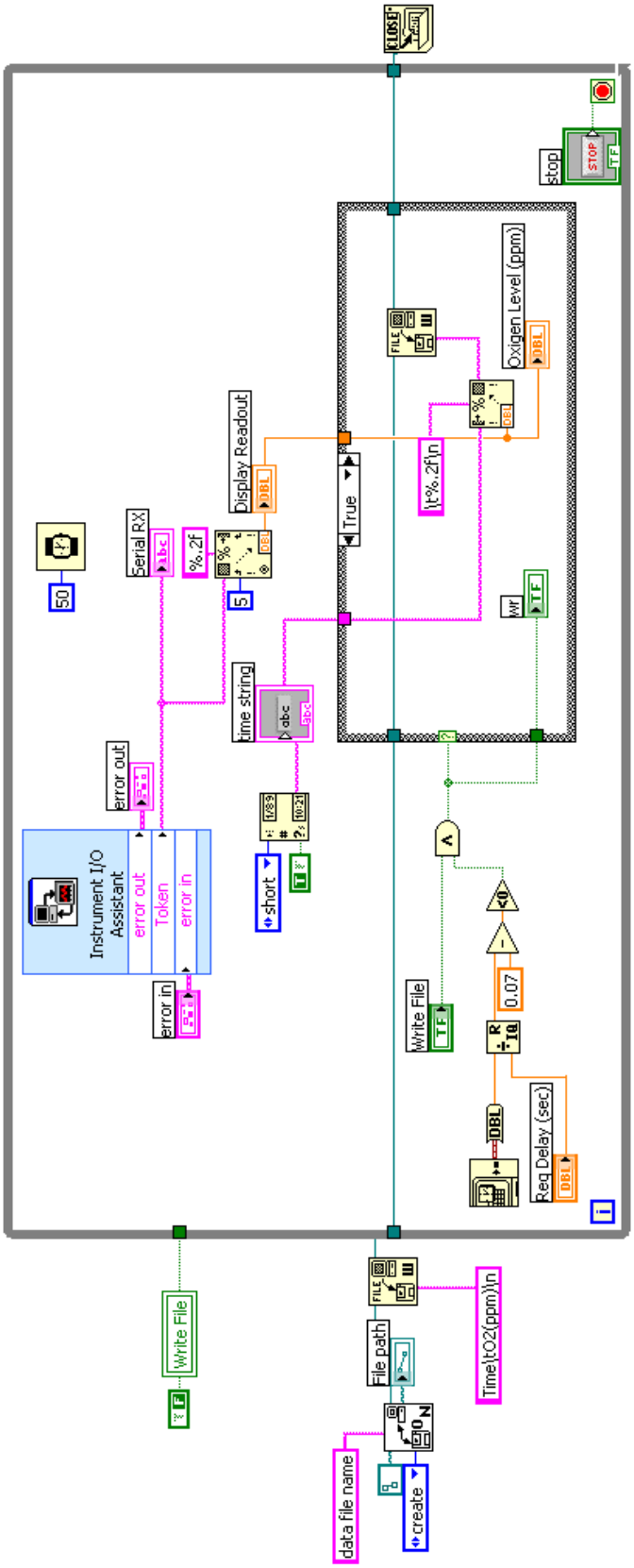

Figure A-4: Lab View Data Acquisition Program for O2 Detection

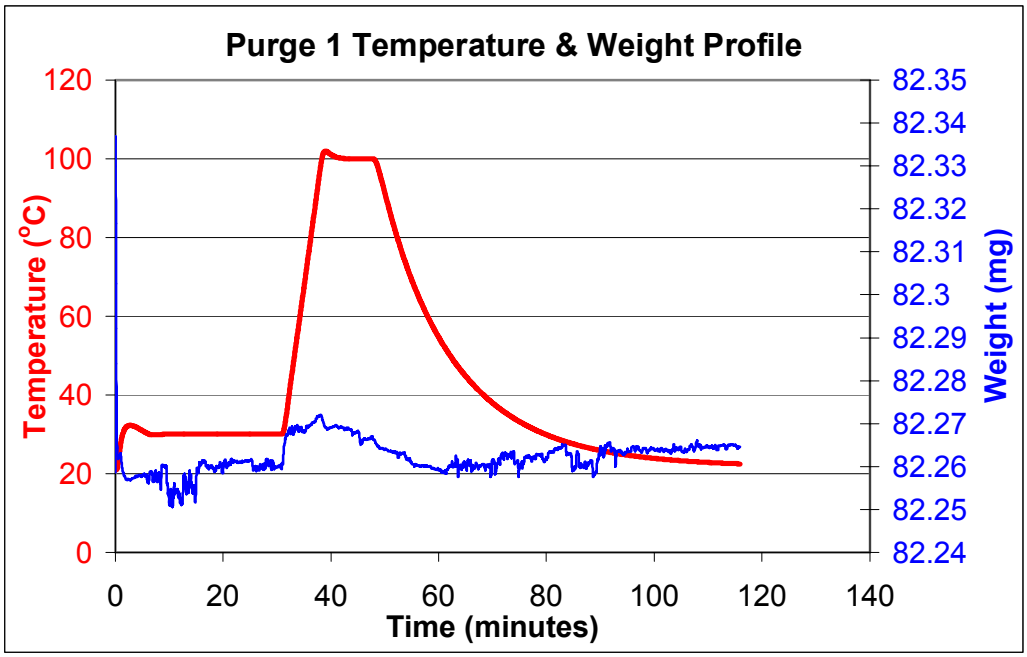

Figure A-5: Test 1 Purge Temperature and Weight Profile

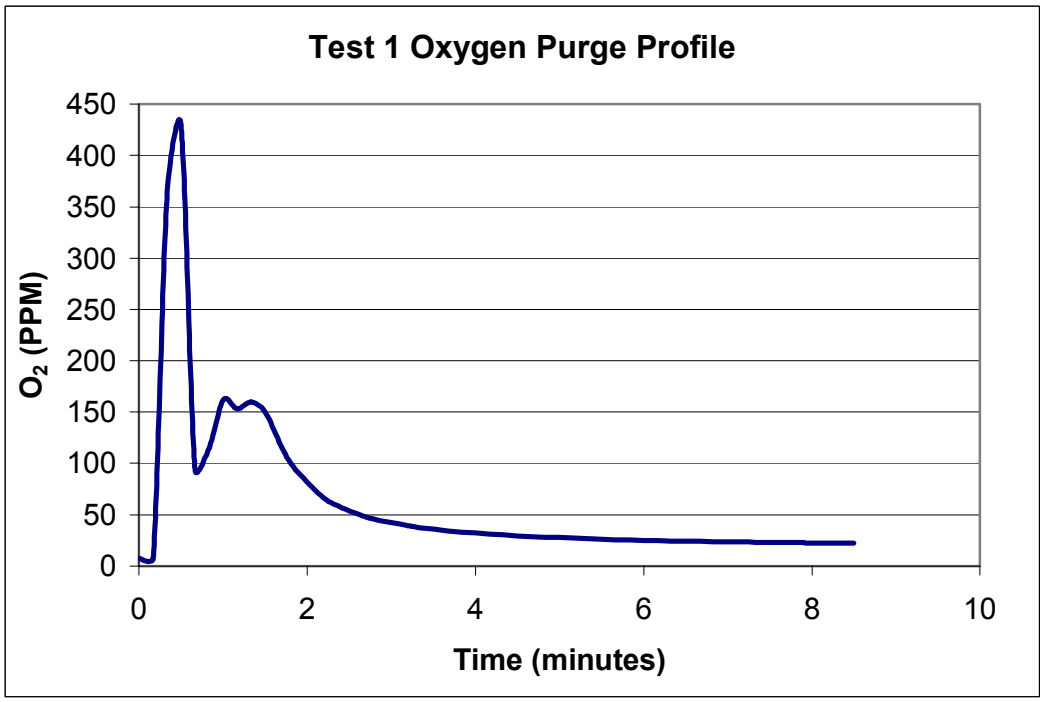

Figure A-6: Test 1 Purge Exhaust Oxygen Concentration Profile

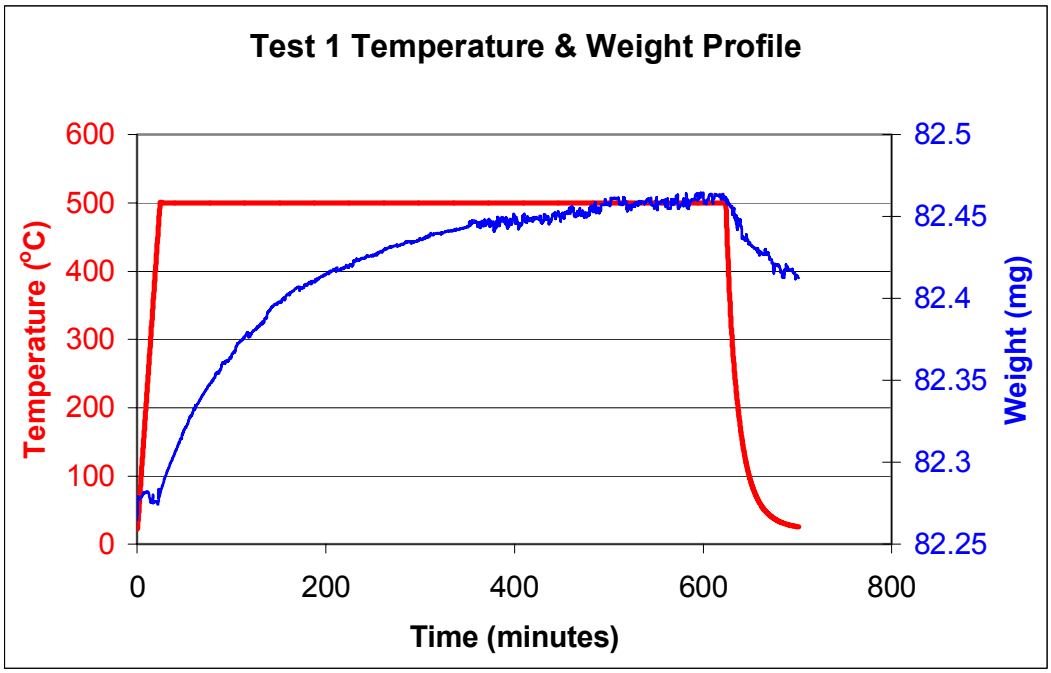

Figure A-7: Test 1 Temperature & Weight Profile

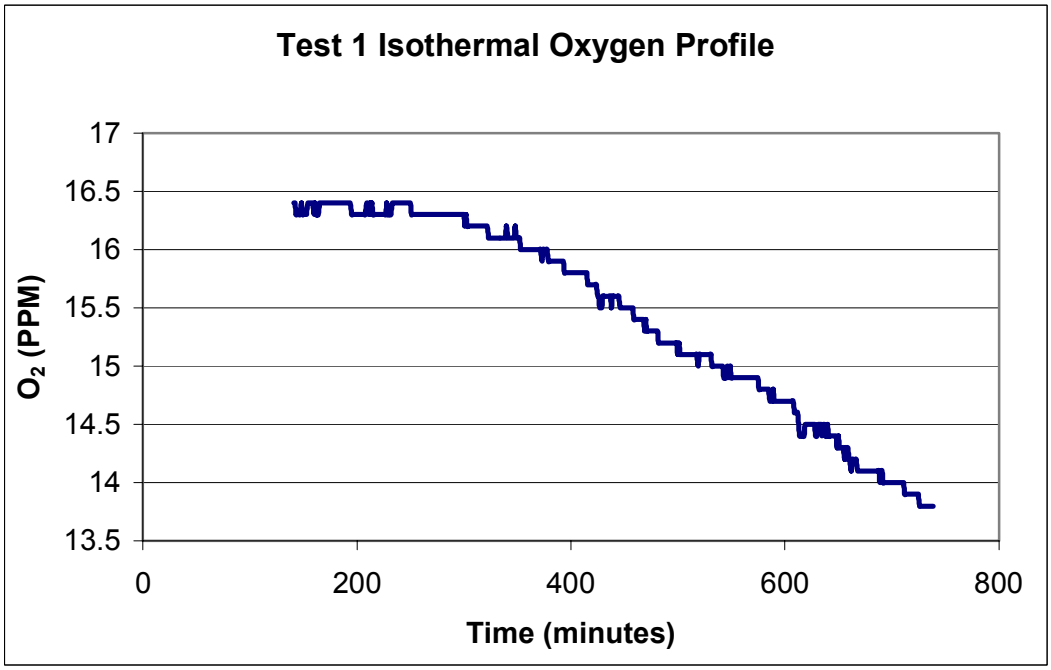

Figure A-8: Test 1 Isothermal Oxygen Concentration Profile

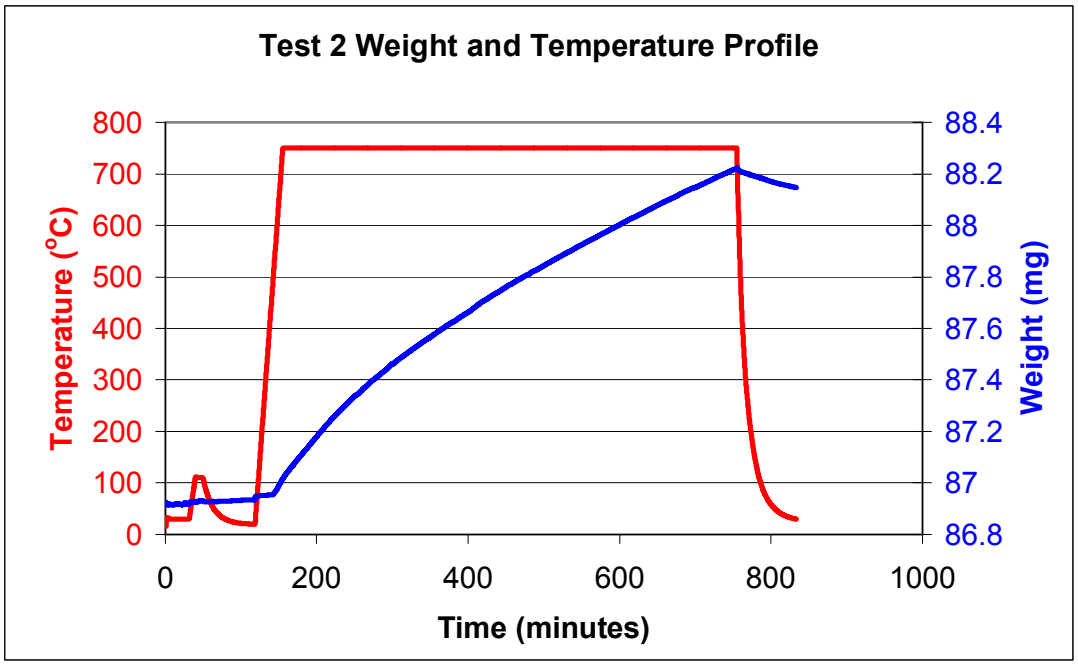

Figure A-9: Test 2 Temperature & Weight Profile

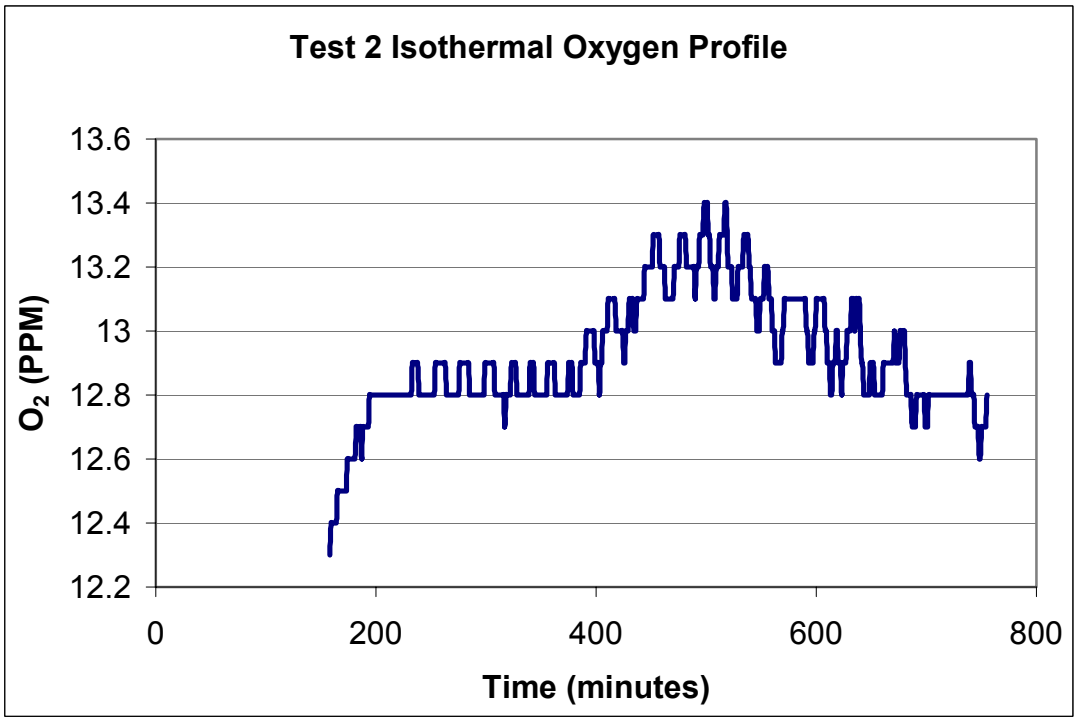

Figure A-10: Test 2 Isothermal Oxygen Concentration Profile

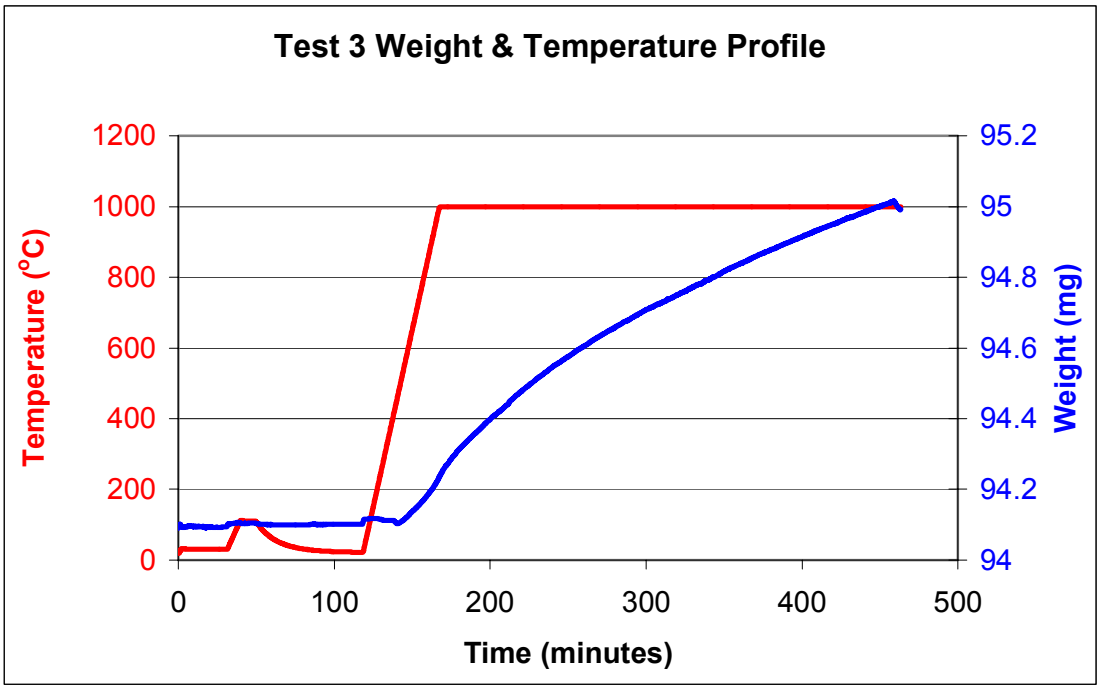

Figure A-11: Test 3 Temperature & Weight Profile

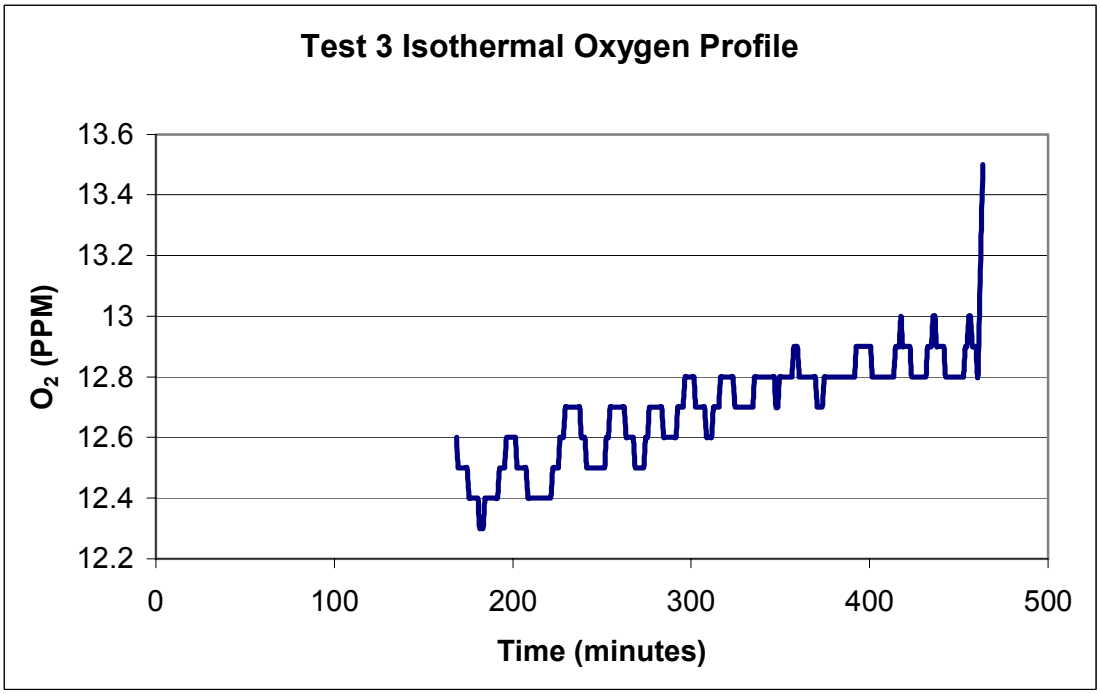

Figure A-12: Test 3 Isothermal Oxygen Concentration Profile

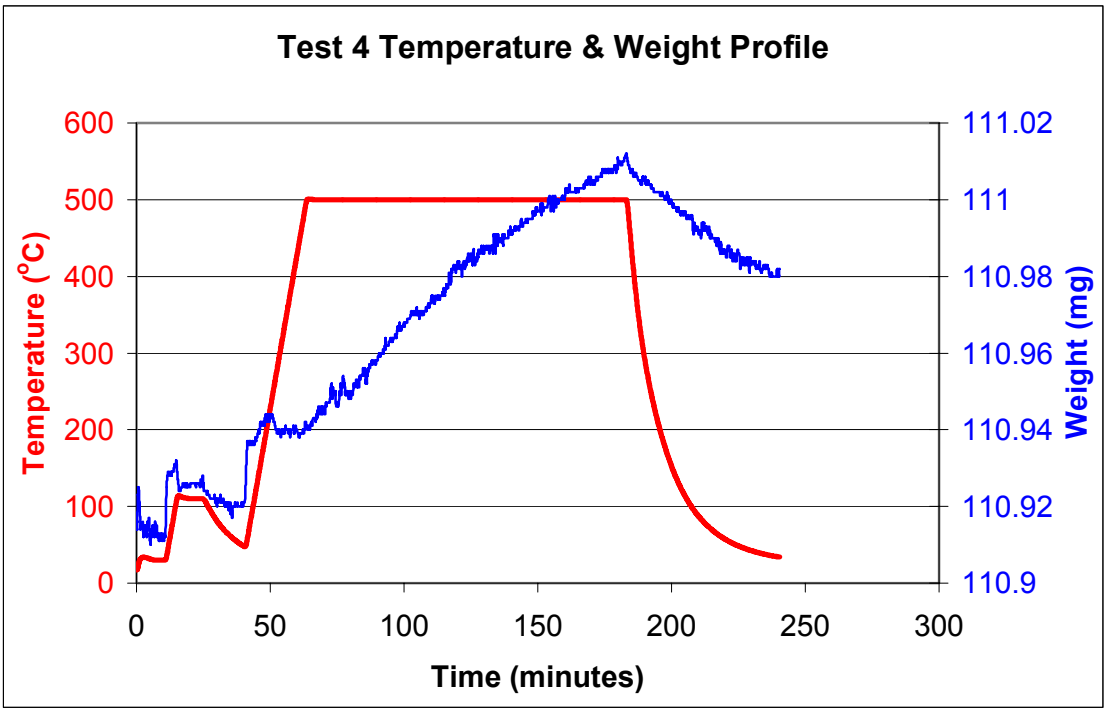

Figure A-13: Test 4 Temperature & Weight Profile

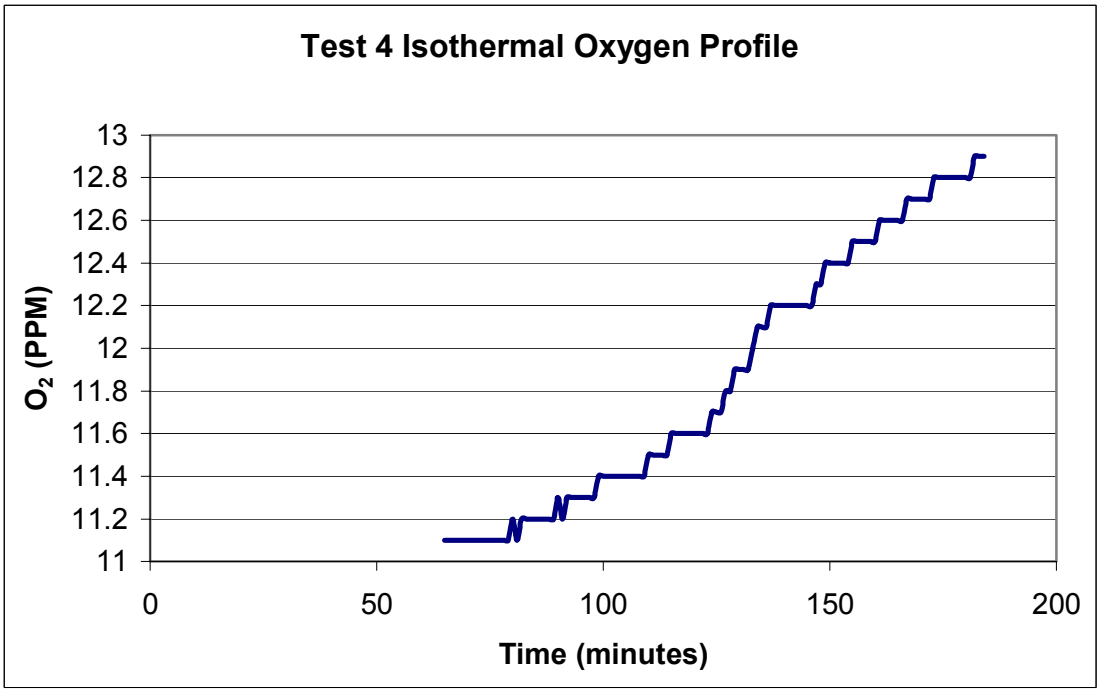

Figure A-14: Test 4 Isothermal Oxygen Concentration Profile

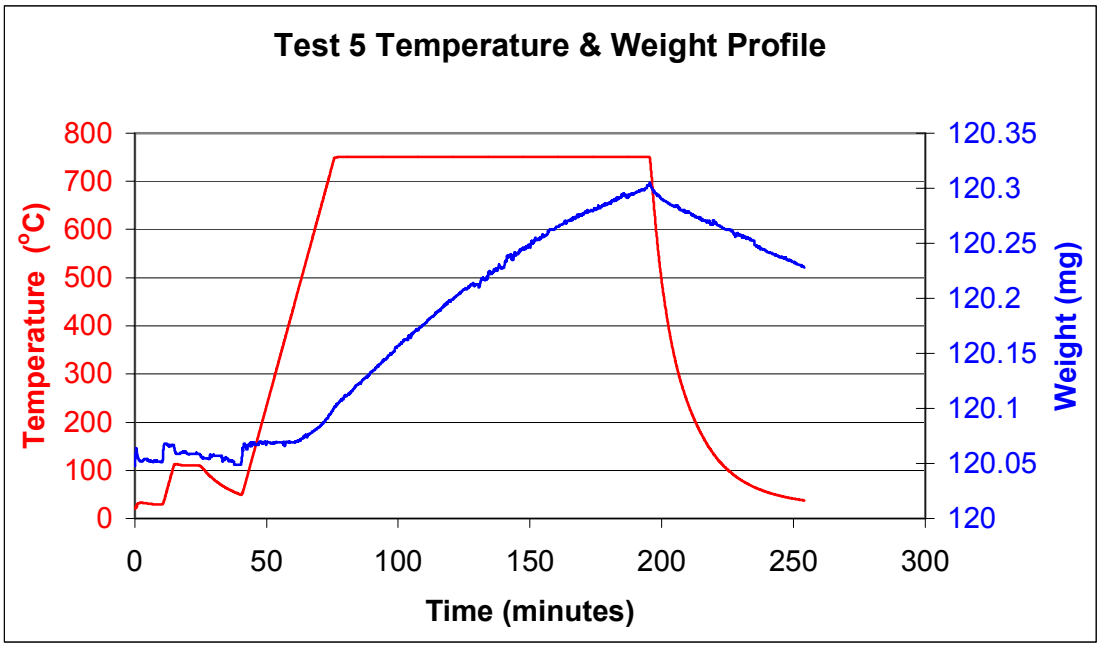

Figure A-15: Test 5 Temperature & Weight Profile

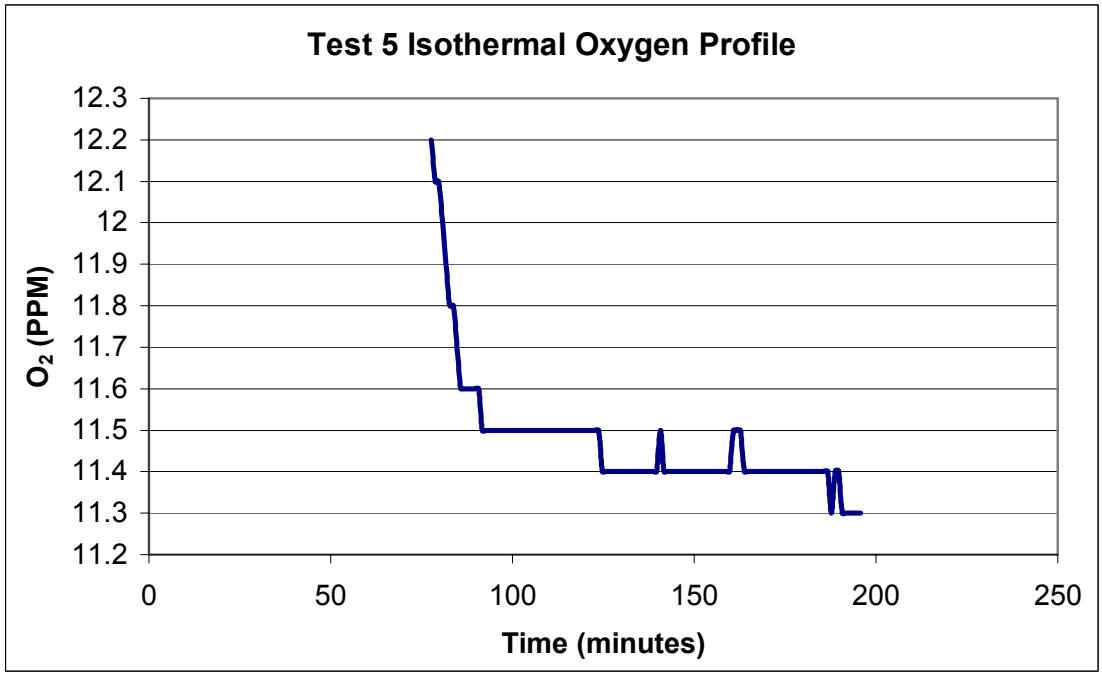

Figure A-16: Test 5 Isothermal Oxygen Concentration Profile

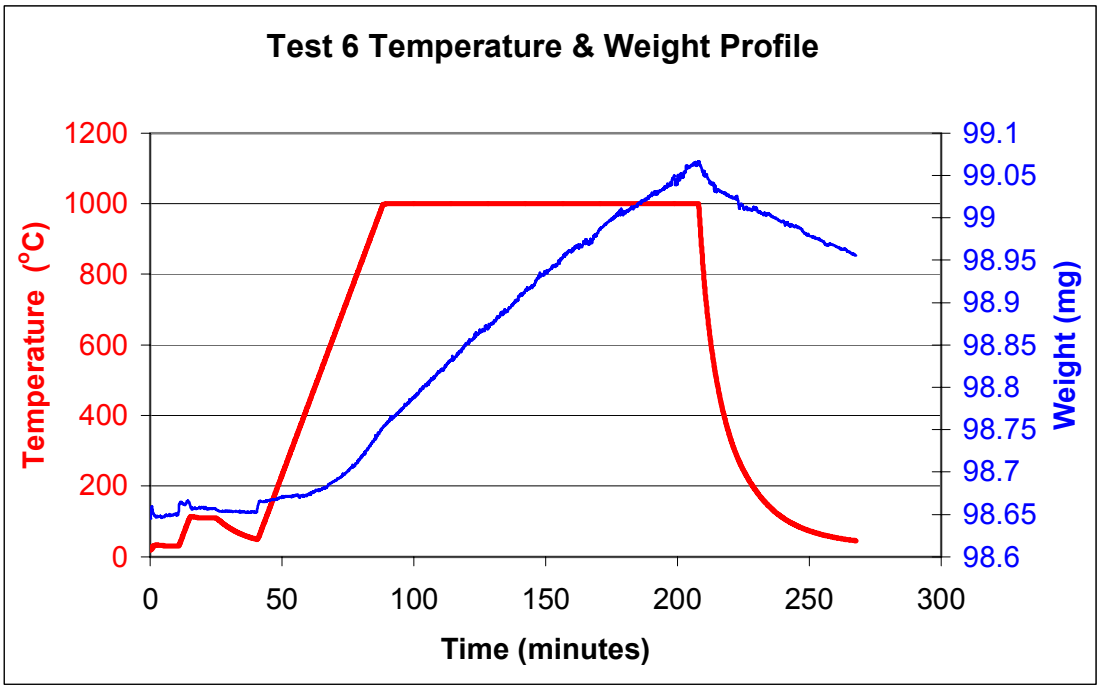

Figure A-17: Test 6 Temperature & Weight Profile

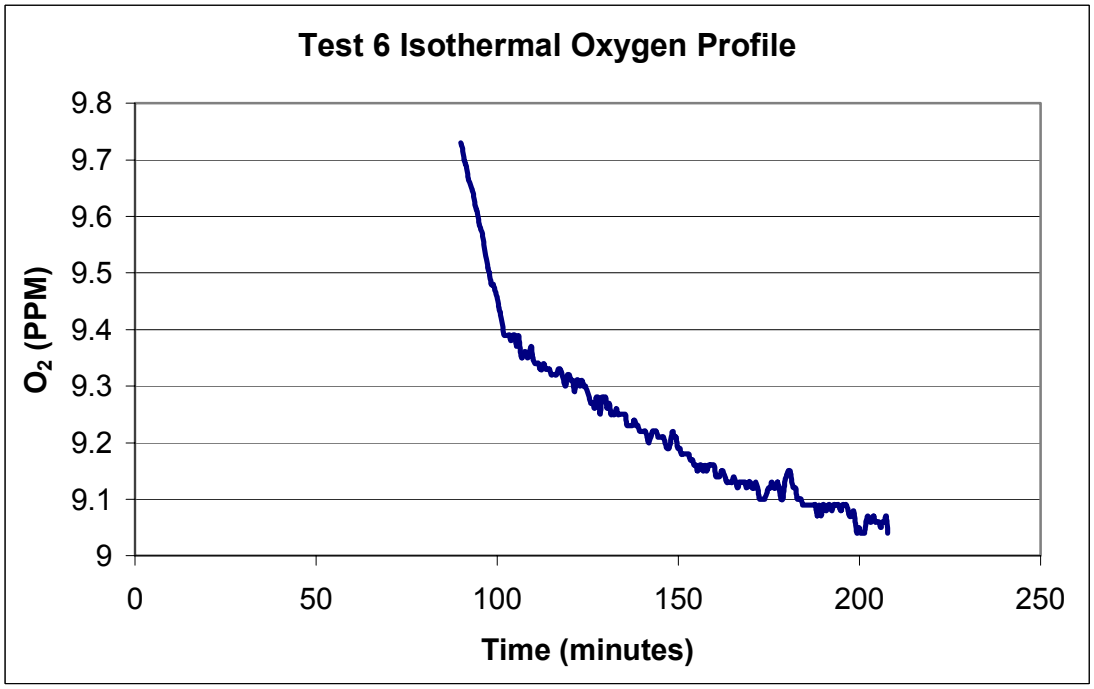

Figure A-18: Test 6 Isothermal Oxygen Concentration Profile

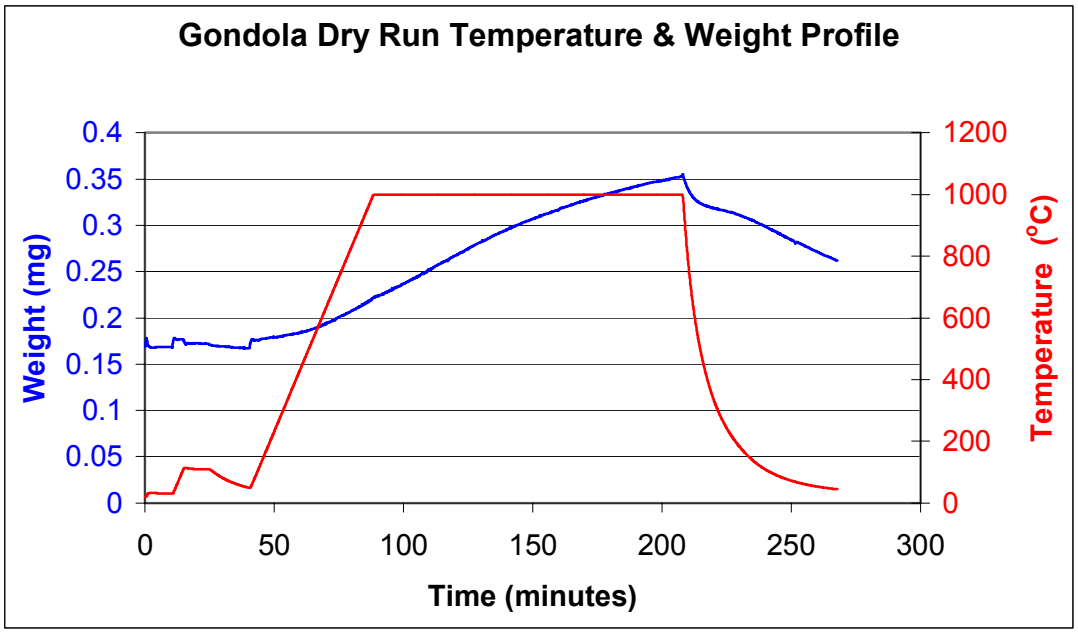

Figure A-19: Gondola Dry Run Temperature & Weight Profile

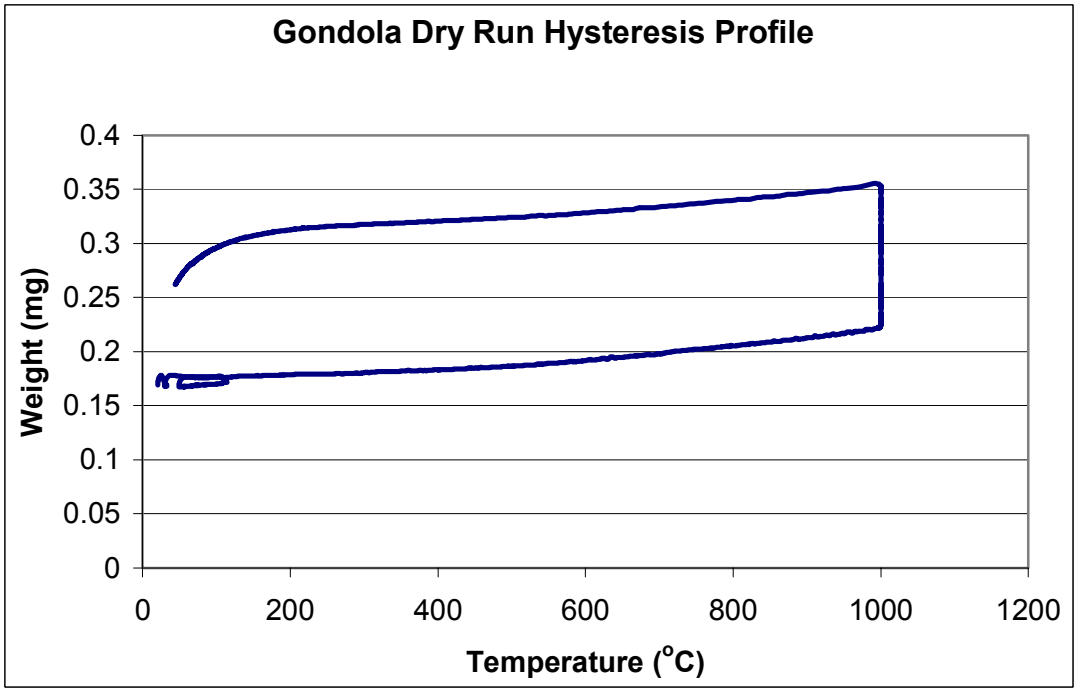

Figure A-20: Gondola Dry Run Hysteresis Profile

REFERENCES

Angelo, Joseph; Buden, David. *Space Nuclear Power*. Orbit Book Company, Inc. 1985.

ASM Metals Handbook, *Properties and Selection of Nonferrous Alloys and Special Purpose Materials,* Vol 2, ASM International, Metals Park, OH, 1990 pp.565-569.

ASM Handbook, *Alloy Phase Diagrams*, Vol 3, ASM International, Metals Park, OH, 1992, pp 308.

ASM Specialty Handbook, *Heat Resistant Materials,* ASM International, Metals Park, OH, 1997, pp 65, 362-377.

ASM Specialty Handbook, *Stainless Steels,* ASM International, Metals Park, OH, 1994, pp 209.

Barsoum, M.W., *Fundamentals of Ceramic*s, McGraw-Hill. 1996

Callister, William D Jr., *Materials Science and Engineering an Introduction,* John Wiley & Sons, Inc, New York, NY, 1999, pp. 540.

DiStefano, J.R., Chitwood, L.D., "Oxidation and it Effects on the Mechanical Properties of Nb-1Zr," in *Journal of Nuclear Materials,* 295, 42 – 48 (2001).

DiStefano, J.R., Hendricks, J.W., "Oxidation of Nb-1Zr in Space System Environments," ORNL/TM-11423, Oak Ridge National Laboratory, 1990.

Incropera, Frank P., and DeWitt, David P., *Fundamentals of Heat and Mass Transfer: Fifth Edition,* John Wiley & Sons, Inc, New York, NY, 2002, pp. 811.

Keeton, Alvin R., Alexion, Chris C., and Bagnall, Chris, "Fabrication of A Niobium 1% Zirconium Containment For SP-100 Primary Lithium System Materials Mass Transfer

Studies," in *Transactions of the 4th Symposium on Space Nuclear Power Systems*, Institute for Space Nuclear Power Studies, Albuquerque, NM, 1987, pp.517-520.

King, Jeffrey C., El-Genk, M.S., "A Review of Refractory Materials for Vapor-Anode AMTEC Cells," in *Proceedings of the Space Technology and Applications International Forum (STAIF 2000)*, edited by M.S. El-Genk, AIP Conference Proceedings No. 504, American Institute of Physics, New York, 2000, pp. 1391-1401.

Kramer, D.P., Ruhkamp, J.D., McNeil, D.C., Mintz, G.V., and Howell, E.I., "Mechanical Testing Studies of Niobium – 1% Zirconium in Association with its Applications as Cell Wall Material in an AMTEC Based Radioisotope Space Power System," in *Proceedings of the 34th Intersociety Energy Conversion Engineering Conference*, Society of Automotive Engineers, Inc., Warendale, PA, 1999, Paper No. 1999-01-2608, pp.611-615.

Lee, William E., Rainforth, W. Mark, *Ceramic Microstructures: Property Control by Processing,* Chapman and Hall Inc, University Press, Cambridge, 1994, pp. 114-117.

Oak Ridge National Laboratories (ORNL), "Multimegawatt Space Nuclear Power Program Structural Materials Data Sheets," (1988), http://www-rsicc.ornl.gov/ANST_site/multimega.pdf, accessed June 12, 2003.

Poston, David I., "Nuclear Design of the SAFE-400 Space Fission Reactor," in *Nuclear News*, American Nuclear Society, La Grange Park, Il, 2002, pp.28-35.

Scheuermann, C.M., Moore, T.J., and Wheeler, D.R., "Preliminary Study of Niobium Alloy Contamination by Transport Through Helium," in *Transactions of the 4th Symposium on Space Nuclear Power Systems*, Institute for Space Nuclear Power Studies, Albuquerque, NM, 1987, pp.103-106.

Schmidt, M.A., and Kania, M.J., "A Review of Diffusion Barrier Technology for Application in SP-100 Fuel Pins," in *Transactions of the 4th Symposium on Space Nuclear Power Systems*, Institute for Space Nuclear Power Studies, Albuquerque, NM, 1987, pp. 319-322.

Sholtis, Joseph A., et al., "U.S. Space Nuclear Safety: Past, Present, and Future," in *A Critical Review of Space Nuclear Power and Propulsion 1984 – 1993,* American Institute of Physics, New York, 1994, pp. 285.

Tietz, Thomas E. and Wilson, J. W., *Behavior and Properties of Refractory Metals,* Stanford University Press, 1965, pp. 102 – 151.

Wah Chang Corporation, "Niobium," (2003), http://www.wahchang.com/WahChang/pages/products/data/niobium/Niobium.pdf, accessed June 23, 2003.

Yu W., Chen S., Zee R.H., and B.A., "Creep of Nb –1Zr to Stainless Steel Transition Joint," in *International Trends in Welding Science and Technology,* ASM International, Metals Park, OH, 1993, pp.611-615.